KLOE Note # 209

January 13, 2006

Measurement of $\Gamma(K_S \to \pi^+\pi^-(\gamma))/\Gamma(K_S \to \pi^0\pi^0)$ with 2001-2002 data.

C. Gatti, M. Palutan, T. Spadaro

Laboratori Nazionali di Frascati - INFN

Abstract

A detailed description of a new measurement of the ratio $\mathrm{R}_\mathrm{S}^\pi = \Gamma(\mathrm{K_S} \to \pi^+\pi^-(\gamma))/\Gamma(\mathrm{K_S} \to \pi^0\pi^0)$ is given. We have used a sample of of 410 pb^{-1} acquired during years 2001 and 2002. Respect to the published result, based on 2000 data, we profited of a much more accurate Monte Carlo simulation. This allowed us to improve the systematic error by a factor of three, reaching a total fractional uncertainty of 2.5×10^{-3}. We find $\mathrm{R}_\mathrm{S}^\pi = 2.2555 \pm 0.0012_\mathrm{stat} \pm 0.0021_\mathrm{syst-stat} \pm 0.0050_\mathrm{syst}$, which is in good agreement with our previously published result. The average of KLOE results gives $\mathrm{R}_\mathrm{S}^\pi = 2.2549 \pm 0.0054$.

Contents

1 Introduction

In this section we briefly review the main motivations to a new measurement of $\mathrm{R}_\mathrm{S}^\pi$; then we remind the salient features of the published analysis, and we discuss the critical items to improve the systematic error, which have been addressed in the Monte Carlo simulation we use.

1.1 Motivations for $\mathrm{R}_\mathrm{S}^\pi$

On may 2002 we published a measurement of $\mathrm{R}_\mathrm{S}^\pi$ based on 17 pb^{-1} acquired during year 2000: $\mathrm{R}_\mathrm{S}^\pi = 2.236 \pm 0.003_\mathrm{stat} \pm 0.015_\mathrm{syst}$ [5]. This result was more precise than the previous PDG average [11] and increased by 0.5% the PDG fit result for $\mathrm{BR}(K_S \to \pi^+\pi^-(\gamma))$ [13]. The motivation to repeat this measurement on 2001-2002 data set is two-fold:

- $\mathrm{R}_\mathrm{S}^\pi$ fixes $\Gamma(K_S \to \pi^+\pi^-(\gamma))$ to one part in 10^3 and therefore it is needed to evaluate V_us from the measurement of $\Gamma(K_S \to \pi e\nu)/\Gamma(K_S \to \pi^+\pi^-(\gamma))$, which is performed consistently on the same data set; moreover on the 2001-2002 sample we can profit of a new detailed Monte Carlo simulation, whose improvements allowed us to better understand the main systematic limitations affecting the measurement of $\mathrm{R}_\mathrm{S}^\pi$.

- This is one of the *golden plated* channel to push the study of systematics for high precision measurements in KLOE, because of high statistical reach and the presence of both charged and neutral final states with simple topology.

1.2 The published analysis: a brief reminder

In the published analysis the event selection was based on a clean K_S tagging by time-of-flight identification of K_L interactions in the calorimeter ("K_cr"), with a visible energy above 200 MeV. K_L velocity in the ϕ rest frame was selected in the range $0.195 < \beta^* < 0.2475$, with an absolute tagging efficiency of about 30% ($\sim 3\times10^5$ tagged K_S per pb^{-1}).

The $K_S \to \pi^+\pi^-(\gamma)$ signal was selected by requiring two oppositely charged tracks from the interaction point (IP) with the additional request to be extrapolated to the calorimeter, in order to increase the probability of providing the time-zero (T_0) cluster to the event. The overall acceptance was 0.5697 ± 0.0016. $K_S \to \pi^0\pi^0$ signal was selected by requiring more than two prompt clusters from the IP, with an overall efficiency of 0.8992 ± 0.0018.

Signal selection efficiencies were taken from Monte Carlo, but the trigger and cosmic veto ones, which were extracted directly from data. The ratio of data over Monte Carlo tracking efficiency ($\epsilon_{\rm trk}(\rm data)/\epsilon_{\rm trk}(\rm MC)$) was used to correct the $\pi^+\pi^-$ selection efficiency. The tagging efficiency depends slightly on the K_S-decay mode, because of the event-T_0 determination, which is in most cases displaced by about 2.7 ns in $\pi^+\pi^-$ events. The ratio of $\pi^+\pi^-$ over $\pi^0\pi^0$ tagging efficiencies ratio is evaluated from data, by using the K_L velocity spectrum on subsamples of selected $\pi^+\pi^-$ and $\pi^0\pi^0$ events ($\rm R_{tag} = 0.977 \pm 0.005$). This method gives a systematic error of 0.55%, which is the largest contribution to the total uncertainty.

For this reason, starting from year 2001 the $K_{\rm cr}$ tagging algorithm has been modified in order to accept events in a larger K_L velocity window: $0.17 < \beta^* < 0.28$.

For further details refer to [7].

1.3 Critical items to improve the systematic error

The following items are critical to decrease the systematic error:

- The MC simulation includes the contribution from machine background, that has been inserted on a run-by-run basis, to follow variable running conditions. Both DC and EMC background hits have been superimposed to the simulated event. A correct background simulation is particularly relevant to reproduce the probability for an accidental background cluster to reach the calorimeter prior to a photon or a pion from K_S, thus giving a wrong T_0 for absolute time measurement. This causes a loss both in the photon counting and in the K_L time-of-flight selection.

- The MC simulation better reproduces the interaction of K_L in the calorimeter. Such an improvement allowed us to compute selection efficiencies with inclusion of interference effects between K_S and K_L hemispheres (see next subsection). Moreover we carried on the analysis for three different cuts on the K_L cluster energy: $E_{\text{cr}} = 125, 200$, and $300\ \text{MeV}$, in order to to check the reliability of the efficiency estimates. Last but not least a new method could be introduced to evaluate the ratio R_{tag} between $\pi^+\pi^-$ and $\pi^0\pi^0$ tagging efficiencies (see Sec. 3).

- The MC simulation reproduces machine working point for what concern energy and position of the luminous point. With all the new features included in the simulation, and given the very large statistical abundance available for the analysis, it was straightforward to split the sample into different slices in order to precisely check the stability of the result along the data taking.

1.4 A new K_{cr} simulation

The old K_{cr} simulation was affected by two major problems: it underestimated the energy deposited by K_L interaction in the EMC and it overestimated its time-of-flight. This is shown in Fig. 1, by comparing data and MC spectra for K_{cr} energy and velocity.

Starting from datarec version DBV-18 a new simulation has been implemented for K_L nuclear interaction, providing a much better agreement with data (Fig. 2). The authors (M. Antonelli, T. Spadaro and M. Testa) modified some parameters in the GEISHA generator for nuclear interactions which particularly affected the behaviour of K_L in the low energy range.

To appreciate more quantitatively the improvement that has been reached in the new simulation we report in Tab. 1 the K_{cr} efficiency for data and MC on a sample of events selected by a $K_S \to \pi^0\pi^0$ tag. The cut on the visible K_L energy is moved between 100 and 300 MeV. The kind of agreement we observe between data and MC is not enough good to take the absolute efficiency from the simulation. On the other side it is perfectly suited to rely on the simulated topology in selecting samples for computing the selection efficiencies.

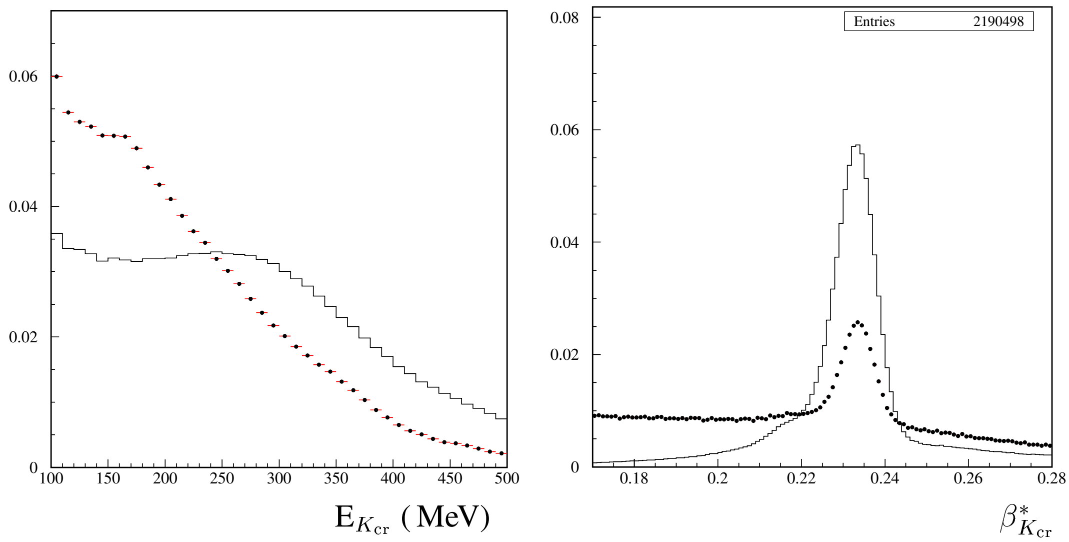

Figure 1: Comparison between data (solid line) and **old** Monte Carlo (dots) for K_{cr} visible energy spectrum (left panel), and K_{cr} beta spectrum (right panel).

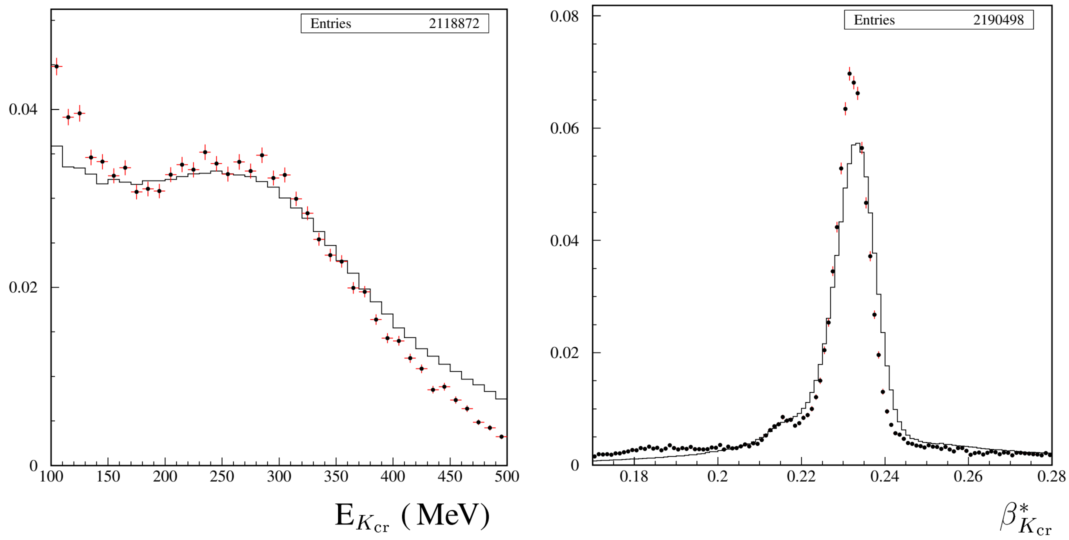

Figure 2: Comparison between data (solid line) and **new** Monte Carlo (dots) for K_{cr} visible energy spectrum (left panel), and K_{cr} beta spectrum (right panel).

ϵ_{cr}	$E_{\rm cr} > 100\,{\rm MeV}$	$E_{\rm cr} > 200\,{\rm MeV}$	$E_{\rm cr} > 300\,{\rm MeV}$
data	0.3350 ± 0.0002	0.2231 ± 0.0002	0.1198 ± 0.0001
old MC	0.1709 ± 0.0001	0.0839 ± 0.0001	0.0407 ± 0.0001
new MC	0.357 ± 0.002	0.228 ± 0.002	0.110 ± 0.002

Table 1: $K_{\rm cr}$ efficiency on events tagged by the identification of $K_S \to \pi^0\pi^0$ decay.

1.5 Interference between K_L and K_S hemispheres

With this new $K_{\rm cr}$ simulation we could use a more precise method in order to compute the average K_S signal acceptance, which is is slightly correlated with the K_L decay kinematics and topology. The left panel of Fig. 3 shows the $K_S \to \pi^+\pi^-(\gamma)$ reconstruction efficiency as a function of the K_L vertex transverse position ($r_{\rm T}$) for all possible K_L final states. A significant drop is visible for charged final states when $r_{\rm T}$ approaches the interaction region. The visible loss of events is due to an interference effect between K_S and K_L tracks in the central region of DC. The reconstruction efficiency is indeed perfectly flat for $K_L \to \pi^0\pi^0\pi^0$ in the whole $r_{\rm T}$ range and for all other final states when reaching the calorimeter surface.

Such an effect plays a role also when K_S signal is selected with a $K_{\rm cr}$ tag; indeed the tag sample contains a small fraction of K_L which decay into charged particles in the DC volume. In the right panel of Fig. 3 the K_L decay $r_{\rm T}$ spectrum is shown for all of the events satisfying the $K_{\rm cr}$ algorithm with $E_{\rm cr}$=125 MeV. The contribution from K_L decays occuring close to the edge of the DC volume is evident. For this reason the K_S signal efficiency given a $K_{\rm cr}$ tag is averaged on the K_L $r_{\rm T}$ spectrum for the selected sample. Such a spectrum is reliably reproduced by the new $K_{\rm cr}$ simulation, which properly takes into account the contribution from both the K_L nuclear interactions and the K_L late decays. The inclusion of the interference effect gives an average efficiency which is 0.1% lower with respect to the plateau value, the one we used in the past.

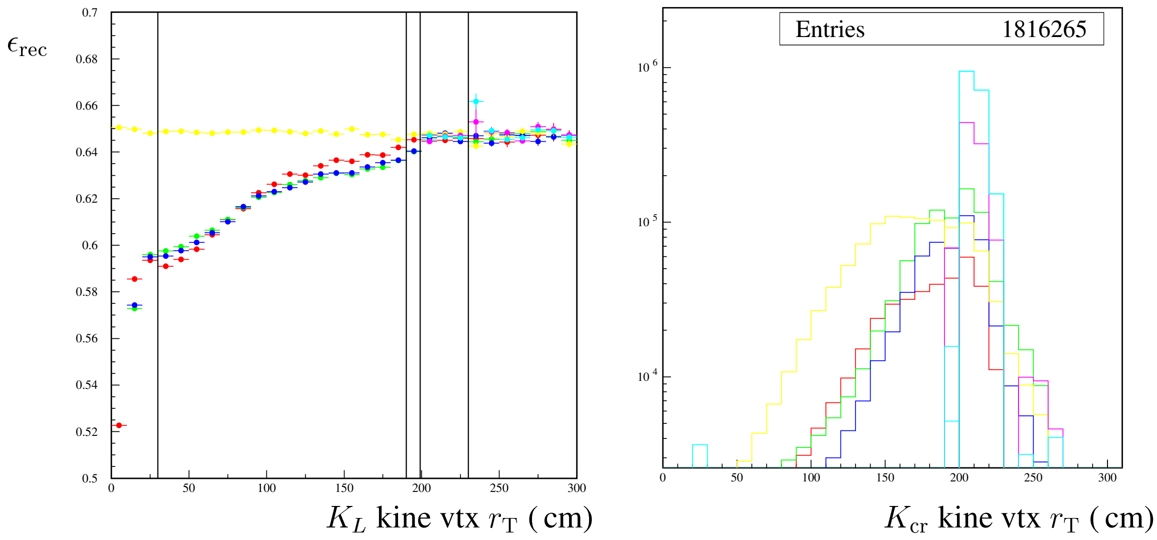

Figure 3: Left panel: efficiency for $K_S \to \pi^+\pi^-(\gamma)$ reconstruction as a function of K_L decay mode and K_L vertex transverse position (cm); right panel: K_L vertex transverse position (cm) for events satisfying the $K_{\rm cr}$ algorithm. K_L final states are reported with different colours: green=K_{e3}, blue=$K_{\mu 3}$, yellow=$\pi^0\pi^0\pi^0$, red=$\pi^+\pi^-\pi^0$, cyan=nuclear, violet=regeneration .

1.6 Data set

Before entering the details of the analysis, a brief remark has to be given on the data set we use. We analyzed $410\mathrm{pb}^{-1}$ acquired during year 2001 and 2002. Data have been divided into 17 periods following the variations of $\sqrt{s}$ and trigger conditions. For a detailed discussion on the data quality criteria we adopted, refer to [4]. Selection efficiencies are evaluated separately for each period, together with the corrections extracted directly from data. This allowed us to get independent results from all of the periods. The list of run intervals is reported in Ref. [4], together with the associated integrated luminosities.

The large event yield we have, allowed us to get a statistical error at the per-mil level for each single period. This gave us the possibility to perform a stringent stability test on our results.

1.7 Outline

In the following sections we describe all of the analysis steps. We will describe in detail what is new respect to the published analysis, while referring to [5],[6],[7],[3],[10],[2] for well established features of our work.

In Sec. 2 the analysis scheme is presented, where a new method is implemented to evaluate the ratio of tagging efficiencies (see also Sec. 3). In Sec. 4 we review the $\pi^0\pi^0$ signal selection and the acceptance evaluation; the study of systematic errors has been greatly improved in this version of the analysis. $\pi^+\pi^-$ selection criteria and acceptance evaluation are almost unchanged respect to the past, and they are discussed in Sec. 5. Trigger, cosmic veto and Filfo efficiency corrections are presented in Sec. 6, Sec. 7 and Sec. 8, respectively. We present the final result in Sec. 10.

2 Analysis scheme

With the introduction of the $K_{\rm cr}$ simulation, we had to change the analysis scheme. The crucial point is the requirement for the event to have a T_0 and the efficiency related to this requirement.

The T_0 is needed to fix the initial time of the event, and the definition of $K_{\rm cr}$ strictly depends on it. As in the past the event T_0 is obtained from the first particle reaching the calorimeter (pions or photons for the events of interest) assuming a velocity $\beta = 1.$. This definition of the interaction time ($T_0^{\rm ev}$ in the following) does not require the K_S decay to be identified. In order to reduce the probability that $T_0^{\rm ev}$ is accidentally determined from a particle due to machine background, we require it to be fixed by a cluster with energy $\mathrm{E_{CL}} > 50\,\mathrm{MeV}$ and distance from the beam line $\rho_{\rm CL} > 60\,\mathrm{cm}$.

Charged pion from $K_S \to \pi^+\pi^-(\gamma)$ arrive at the EMC $\sim 3\,\mathrm{ns}$ later than γ's from π^0 decays. The time $T_0^{\rm ev}$ computed with the assumption above is therefore delayed by one RF period, $T_{\rm RF} \sim 2.7\,\mathrm{ns}$. This results in a $\sim 10\%$ overestimation of the velocity from long-lived kaons accompanied by $K_S \to \pi^+\pi^-(\gamma)$ decays. Therefore, the efficiency for the cut on β^* slighlty depends on the K_S decay mode.

The $T_0^{\rm ev}$ determination not only affects directly the tag efficiency, but it has some consequences also on the way to calculate the signal acceptance given the tag. For $K_S \to \pi^+\pi^-(\gamma)$ events the $T_0^{\rm ev}$ efficiency is indeed evaluated on data after the tracks have been associated to calorimeter clusters. The geometrical acceptance for having two tracks from IP is instead evaluated from MC before the $T_0^{\rm ev}$ requirement (these two efficiencies are clearly correlated). In the old MC simulation the $K_{\rm cr}$ was selected by simply requiring a K_L vertex (from MC truth) in the calorimeter. No explicit $T_0^{\rm ev}$ was needed for this, so that the two-track acceptance given the tag was evaluated independently from it. With the new simulation we could in priciple apply the same $K_{\rm cr}$ algorithm as in data, which requires a $T_0^{\rm ev}$. This obviously create a conflict in the previously described analysis flow.

To overcome this problem we use the true interaction time from MC truth ($T_0^{\rm true}$) when applying the $K_{\rm cr}$ algorithm on MC ($K_{\rm cr}^{\rm true}$). All of the events are then classified depending on whether they satisfy (cr) or not ($\overline{cr}$) $K_{\rm cr}^{\rm true}$. All the MC efficiencies are evaluated separately for cr and $\overline{cr}$ events, and then combined together using the following formula, giving the selection efficiency for both $\pi^+\pi^-$ and $\pi^0\pi^0$ events:

$$\epsilon_{\rm sel} = \left[\epsilon_{cr} a_{cr} \sum_n f_n P_n^{in} + (1-\epsilon_{cr}) a_{\overline{cr}} \sum_n f_n P_n^{out} \right] \epsilon_{\rm trg} \epsilon_{\rm CV} \epsilon_{\rm FILFO}, \tag{1}$$

where

- ϵ_{cr} is the efficiency for $K_{\rm cr}^{\rm true}$ algorithm, taken from MC; although the simulation does not reliably reproduce the absolute value of this efficiency, nevertheless it does if the **ratio** between $\pi^+\pi^-$ and $\pi^0\pi^0$ $K_{\rm cr}$ efficiencies is considered (Sec. 3).
- a_{cr} ($a_{\overline{cr}}$) is the acceptance given (vetoed) $K_{\rm cr}^{\rm true}$, including the efficiency for producing a $T_0^{\rm true}$ cluster. The signal acceptance is slighlty correlated with the K_L decay kinematics and topology, thus leading to a difference between a_{cr} and $a_{\overline{cr}}$. These acceptances are taken from MC, data-driven corrections are implemented for tracking and clustering efficiencies (Sec. 4 and Sec. 5).
- f_n is the $T_0^{\rm ev}$ spectrum, *i.e.* the fraction of events in which $T_0^{\rm ev}$ is shifted by $n \times T_{\rm RF}$ with respect to the true time of collision. It is extracted from data (Sec. 3).
- P_n^{in} is the probability that, given a $K_{\rm cr}^{\rm true}$ found, a $K_{\rm cr}$ tag is found as well in presence of a $n \times T_{\rm RF}$ shift of the $T_0^{\rm ev}$ determination. It is taken from data (Sec. 3).
- P_n^{out} is the probability that, without a $K_{\rm cr}^{\rm true}$ found, a $K_{\rm cr}$ tag is found instead in presence of a $n \times T_{\rm RF}$ shift of the $T_0^{\rm ev}$ determination. It is taken from data (Sec. 3).
- $\epsilon_{\rm trg}$, $\epsilon_{\rm CV}$ and $\epsilon_{\rm FILFO}$ are the efficiencies for trigger, cosmic veto and for the offline background filter (FILFO). All of these efficiencies have been evaluated on data samples (Sec. 6, Sec. 7 and Sec. 8).

All of the efficiencies are to intended as conditional probabilities with respect to the previous step in the analysis, according to the order in which they appear in Eq.1.

Letting $A = \sum_n f_n P_n^{in}$ and $B = \sum_n f_n P_n^{out}$, the combination $\epsilon_{cr} A + (1-\epsilon_{cr}) B$ in Eq. 1 gives the new evaluation of the tagging efficiency. We remark again that ϵ_{cr} is the probability for a $K_{\rm cr}$ to be selected with $T_0^{\rm true}$ while A and B terms account for the relative modification in the $K_{\rm cr}$ probability due to errors in the $T_0^{\rm ev}$ evaluation.

To give a flavour of the efficiencies we have to deal with, we report in Tab. 2 typical values (without erros) for all of the quantities that appear in Eq. (1). Due to the smallness of the ratio $B(\pi\pi)/A(\pi\pi)$, the B terms account for a few per mil correction only in the selection efficiency. The ratio of $\pi^+\pi^-$ and $\pi^0\pi^0$ selection efficiencies calculated with Eq. 1 includes the old definition of the ratio of tagging efficiencies $\rm R_{tag}$, if the assumption $a_{cr} = a_{\overline{cr}}$ is made.

	ϵ_{cr}	a_{cr}	A	B	$\epsilon_{\rm trg}$	$\epsilon_{\rm CV}$	$\epsilon_{\rm FILFO}$
$\pi^+\pi^-$	0.311	0.618	0.964	0.0035	0.985	0.965	0.0001
$\pi^0\pi^0$	0.310	0.893	1.0	0.0	0.999	0.963	0.0002

Table 2: Typical values for the efficiencies quoted in Eq. 1; a cut E($K_{\rm cr}$) > 125 MeV has been used.

The validity of the scheme used to factorize the efficiencies has been tested on MC. All of the terms contributing to $\epsilon_{\rm sel}$ in Eq. 1 have been evaluated from simulated events, applying for the efficiencies the same methods used for data. Performing the selection as in data and using the calculated efficiencies we get in the end $\rm R_S^{\pi}$=2.192(1), reproducing the value at Geanfi input (2.1915) within the error.

The number of selected $\pi^+\pi^-$ and $\pi^0\pi^0$ events $N(i)$ and the corresponding selection efficiencies $\epsilon_{\rm sel}(i)$ are combined according to the following equation:

$$\frac{\mathrm{BR}(K_S \to \pi^+\pi^-(\gamma))}{\mathrm{BR}(K_S \to \pi^0\pi^0)} = \frac{N(\pi^+\pi^-)}{N(\pi^0\pi^0)} \times \frac{C(\pi^+\pi^-)}{C(\pi^0\pi^0)} \frac{\epsilon_{\rm sel}(\pi^0\pi^0)}{\epsilon_{\rm sel}(\pi^+\pi^-)}, \tag{2}$$

where $C(i)$ is the purity of the selection for channel i, as evaluated from MC.

3 Tag efficiency (ϵ_{cr}, f_n, P_n^{in}, P_n^{out})

In this section we first discuss the method to extract from data the distributions of f_n, P_n^{in}, P_n^{out}(Sec. 3.1 and 3.2). Then we will address the systematic error connected to the evaluation of $A = \sum_n f_n P_n^{in}$ and $B = \sum_n f_n P_n^{out}$ (Sec. 3.3). Section 3.4 will be devoted to the systematic error on MC evaluation of $\epsilon_{cr}(\pi^+\pi^-)/\epsilon_{cr}(\pi^0\pi^0)$.

3.1 Extraction of f_n

The $T_0^{\rm ev}$ bunch population (f_n) is calculated by normalizing to the number of entries the spectrum of the difference between $T_0^{\rm ev}$ (from the fastest cluster in the hypothesis $\beta = 1$) and the true collision time, $T_0^{\rm true}$. This has to be evaluated for both $\pi^+\pi^-$ and $\pi^0\pi^0$ events **after** the selection requests have been applied. We developed a method to extract these spectra directly from data.

For the charged case we select a $K_S \to \pi^+\pi^-(\gamma)$ decay vertex close to the IP compatible with kaon invariant mass. Then we require the two charged pions to be associated to clusters and we use for each pion the calorimeter time, the pion track length and momentum informations to get an estimate $T_0(\pi)$ of the true collision time $T_0^{\rm true}$. To increase the robustness of our estimate, we require that $T_0(\pi_1) = T_0(\pi_2)$. The spectrum of the difference ΔT_0 between $T_0^{\rm ev}$ and $T_0(\pi)$ is shown in Fig. 4 for data and MC events. As expected, $T_0^{\rm ev}$ overestimates the true collision times in $\sim 97\%$ of the events. This is because the hypothesis $\beta = 1$ made by the $T_0^{\rm ev}$ algorithm always underestimates the pion time of flight. The negative tail of the spectrum is dominated by $T_0^{\rm ev}$'s from machine background hits. A peculiar structure is visible there, with contiguous bunch positions having very different populations. This is due to the filling structure of the machine orbit, which had during all 2001 and 2002 data taking periodicity 5.4 ns instead of 2.7 ns. The ratio between contiguous bunches is not well reproduced by MC, but a good agreement with data is obtained if they are grouped together. This is shown in Fig. 5, where the $\Delta_{\rm bunch} = \Delta T_0/T_{\rm bunch}$ spectrum is shown for data (black dots) and MC. For MC events we evaluated $\Delta_{\rm bunch}$ with the same method used for data (red dots) and using MC truth for the collision time (blue dots). This demonstrates that our method for estimating the

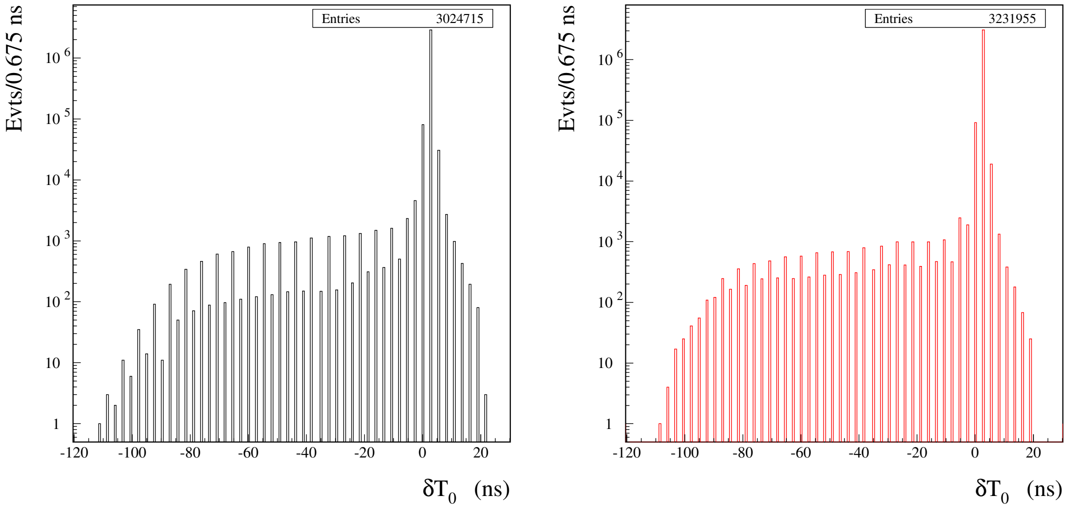

Figure 4: ΔT_0 spectrum for $K_S \to \pi^+\pi^-(\gamma)$ events; data on the left panel, MC events on the right.

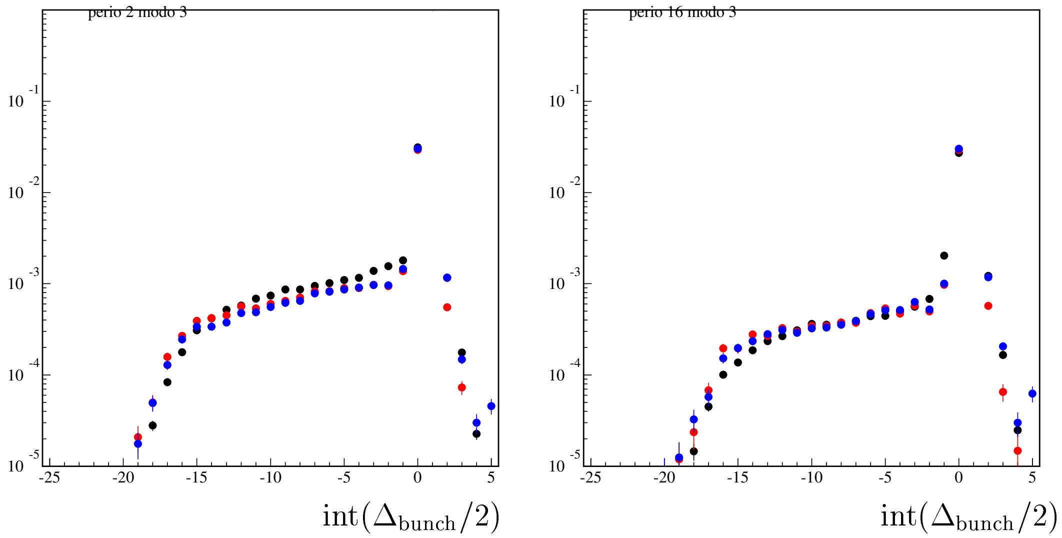

Figure 5: $\Delta_{\rm bunch}$ spectra for data (black), MC-method (red), MC truth (blue); each bin in the plot corresponds to two contiguous bunches; 2001 data on the left panel, 2002 on the right.

$T_0^{\rm ev}$ spectrum does not introduce a relevant bias (see Sec. 3.3).

For $\pi^0\pi^0$ events the situation is simpler, because the request of having at least 3-prompt clusters is fulfilled only if $T_0^{\rm ev} = T_0^{\rm true}$. Therefore $f_n = 0$ for each $n \neq 0$. This is confirmed by studying a sample of $K_S \to \pi^0\pi^0$ events given a $K_L \to \pi^+\pi^-\pi^0$ tagging decay. Even if prompt clusters are selected by using $T_0^{\rm ev}$, these events provide an independent determination of T_0 from the K_L decay chain, $T_0(K_L)$. In the left panel of Fig. 6 we show for MC events the spectra of $(T_0^{\rm true} - T_0^{\rm ev})/T_{\rm RF}$ (blue) and $(T_0(K_L) - T_0^{\rm ev})/T_{\rm RF}$ (red). As expected the $T_0^{\rm ev}$ respect to which the prompt clusters have been found is always the correct one. On the other side the $T_0(K_L)$ is displaced by one bunch in 5×10^{-3} of the cases. This is true also for data, as it is confirmed by the right panel of Fig. 6. The spectra of $(T_0(K_L) - T_0^{\rm ev})/T_{\rm RF}$ are there shown for data (black) and MC (red), together with the MC distribution of $(T_0(K_L) - T_0^{\rm true})/T_{\rm RF}$ (blue).

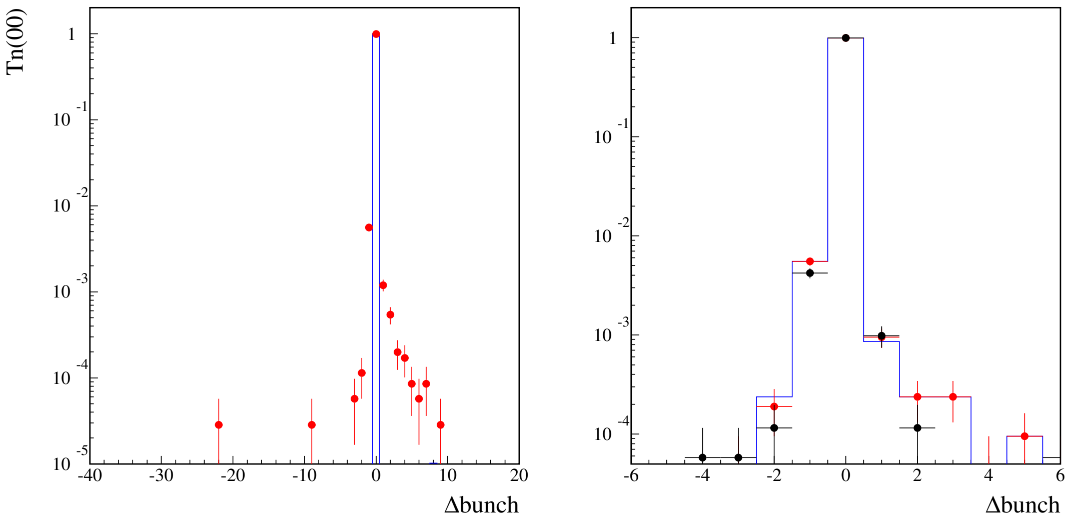

Figure 6: ΔT_0 spectra for $K_S \to \pi^0\pi^0$, $K_L \to \pi^+\pi^-\pi^0$ events: on the left panel $(T_0^{\rm true} - T_0^{\rm ev})/T_{\rm RF}$ (blue) and $(T_0(K_L) - T_0^{\rm ev})/T_{\rm RF}$ (red) for MC events; on the right panel $(T_0(K_L) - T_0^{\rm ev})/T_{\rm RF}$ for data (black) and MC (red), $(T_0(K_L) - T_0^{\rm true})/T_{\rm RF}$ for MC (blue).

A different item is represented by the evaluation of the $\pi^0\pi^0$ signal loss due to a wrong $T_0^{\rm ev}$ from accidental clusters or from the K_S photons themselves. This effect affects directly the acceptance computation, and it will be addressed in Sec. 4.2 and Sec. 4.4.

3.2 Extraction of P_n^{in} and P_n^{out}

To evaluate the P_n^{in} and P_n^{out} probabilities we use a subsample of events tagged by a reconstructed $K_S \to \pi^+\pi^-(\gamma)$ or $K_S \to \pi^0\pi^0$ decay giving the correct T_0 identification, $T_0(K_S)$. The tag we used for $\pi^+\pi^-$ events is described in the previous section. To select $\pi^0\pi^0$ events we required four prompt clusters selected to fit the kinematics of $K_S \to \pi^0\pi^0$ decay.

Given the tag we divide the events into two samples, depending on whether a $K_{\rm cr}$ is found respect to $T_0(K_S)$ or not. On the first sample we then evaluate which is the probability P_n^{in} to **still** find the $K_{\rm cr}$ when moving the T_0 by n bunches respect to $T_0(K_S)$. On the other sample we evaluate instead the probability P_n^{out} to find a $K_{\rm cr}$ **thanks** to a T_0 n-bunch shift. In Fig. 7 the P_n^{in} probabilities are shown for $\pi^+\pi^-$ and $\pi^0\pi^0$ events, for data and MC. For MC events we evaluated P_n^{in} with the same method used for data and using MC truth for the collision time. The two values of P_n^{in} for MC events agree within the errors. The same comparison is shown for P_n^{out} in Fig. 8.

3.3 Evaluation of $A(\pi\pi)$ and $B(\pi\pi)$

In the previous sections we have shown how to extract f_n, P_n^{in} and P_n^{out} from data in unbiased way. From these we can evaluate $A = \sum_n f_n P_n^{in}$ and $B = \sum_n f_n P_n^{out}$. Given the f_n spectrum of $\pi^0\pi^0$ selected events (Sec. 3.1) we get $A(\pi^0\pi^0) = 1$ and $B(\pi^0\pi^0) = 0$. The systematic error we estimate on this assumption will be discussed in the following.

The results for $\pi^+\pi^-$ events are reported in Tab. 3 for period #10 of 2002 data taking, for the three different cuts on $K_{\rm cr}$ energy separately. Note that the lowest cut has been raised from 100 to 125 MeV, as required by the analysis on K_S semileptonic decay [4]. As expected $A(\pi^+\pi^-)$ increases with $K_{\rm cr}$ energy. The tails of the β^* spectrum are indeed suppressed by increasing the energy cut, thus reducing the probability of falling out of acceptance given a wrong T_0.

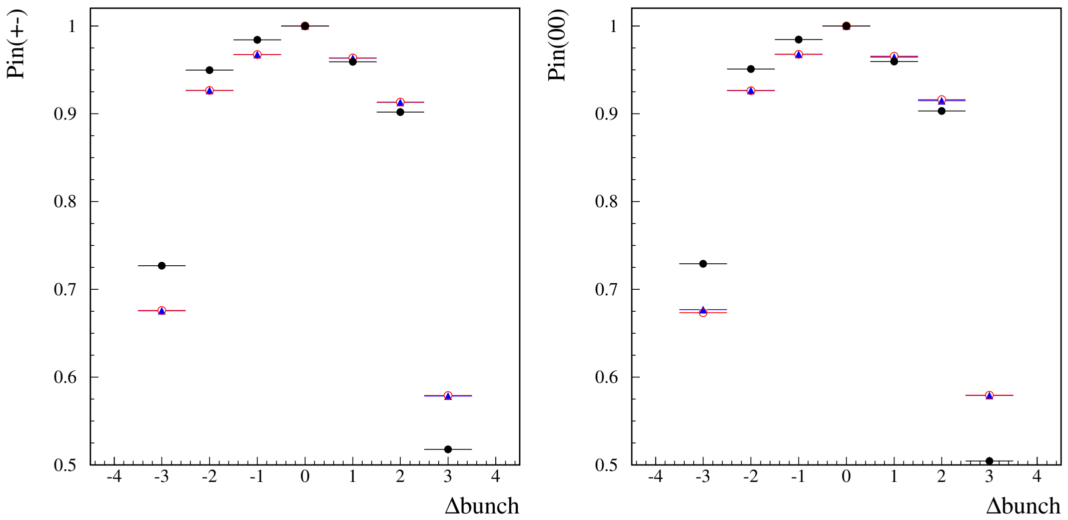

Figure 7: P_n^{in} for $\pi^+\pi^-$ (left panel) and $\pi^0\pi^0$ (right panel) events: data = black, MC-method = red, MC-truth = blue; $P_0^{in} = 1$ by definition.

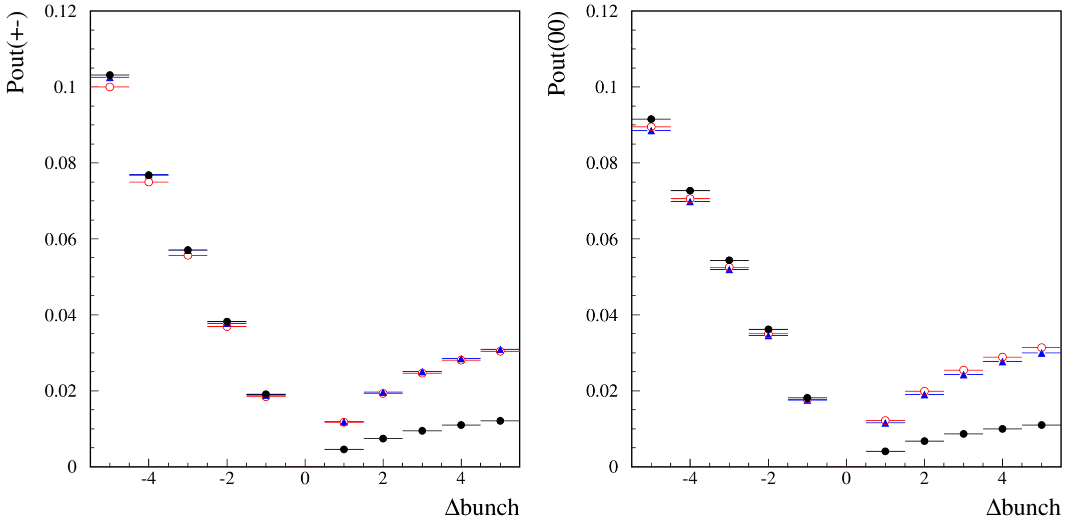

Figure 8: P_n^{out} for $\pi^+\pi^-$ (left panel) and $\pi^0\pi^0$ (right panel) events: data = black, MC-method = red, MC-truth = blue; $P_0^{out} = 0$ by definition.

	A	B
$E_{\rm cr} > 125\,\rm MeV$	0.9634(1)	0.0034489(6)
$E_{\rm cr} > 200\,\rm MeV$	0.9866(1)	0.0016675(1)
$E_{\rm cr} > 300\,\rm MeV$	0.9933(1)	0.00071563(3)

Table 3: Values of A and B for period #10, that belongs to 2002 data taking.

The value of $A(\pi^+\pi^-)$ with $E_{\rm cr} > 125\,\rm MeV$ is shown in Fig. 9 as a function of the data taking period. In principle the fact we use subsamples of events to estimate the f_n

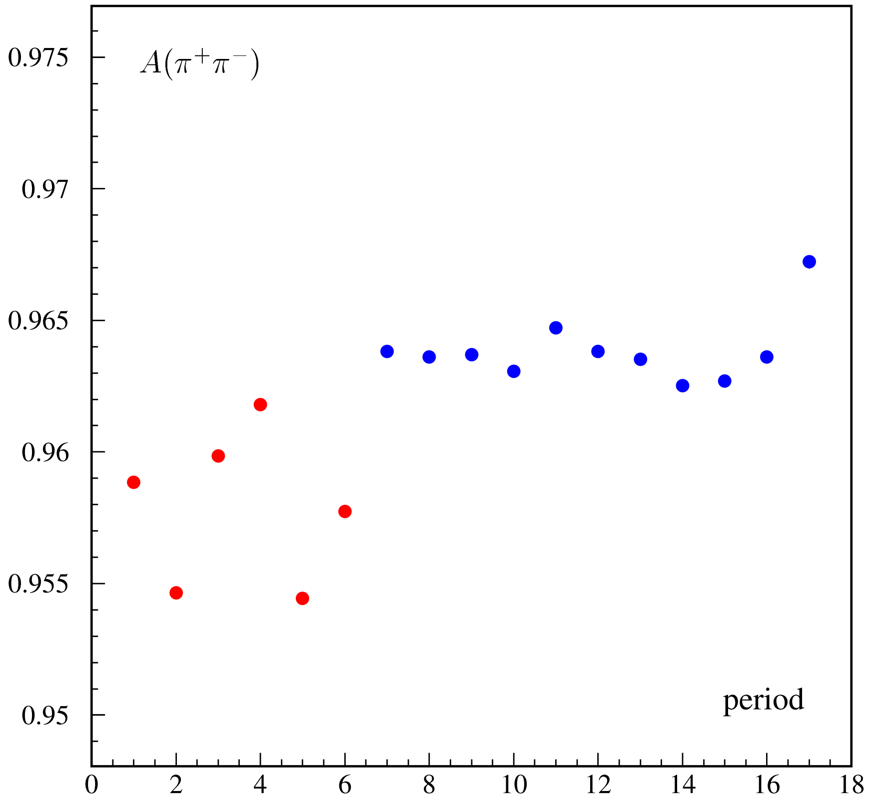

Figure 9: $A(\pi^+\pi^-)$ as a function of the data taking period ($E_{\rm cr} > 125\,\rm MeV$).

spectrum could introduce a bias to the evaluation of A and B. This has been studied on MC events by calculating the ratio $R_1 = A_{\rm MC}^{\rm true}/A_{\rm MC}^{\rm method}$, where $A_{\rm MC}^{\rm true} = \sum_n f_n^{true} P_n^{in,true}$ is the correction evaluated from MC truth and $A_{\rm MC}^{\rm method}$ is evaluated as in data. A better definition of the bias (R_2 in the following) is achieved by replacing in the previous calculation the P_n^{in} probability from MC with the one evaluated on data. R_1 and R_2 have both been calculated and are shown for $\pi^+\pi^-$ events in Fig. 10 for all of the $K_{\rm cr}$ energy cuts. They are consistent with each other. The average value of the bias estimate at 125 MeV $K_{\rm cr}$ energy cut is 0.9996, with an RMS of 0.5×10^{-3}. A similar result is obtained at higher energy. In the end we apply to the value of $A(\pi^+\pi^-)$ calculated on each period the corresponding R_2 correction factor. We assume as a systematic error the difference between results obtained with and without applying this correction. The fractional systematic error is $\sim 0.25 \times 10^{-3}$ for $E_{\rm cr} = 300\,{\rm MeV}$. Given the small value of $B(\pi^+\pi^-)$ we don't apply any correction on it. For $\pi^0\pi^0$ events we use a similar comparison with MC truth to give a systematic error on the assumption $A(\pi^0\pi^0) = 1$. To this purpose we first compute $A(\pi^0\pi^0)$ by using the f_n and P_n^{in} spectra from $K_L \to \pi^+\pi^-\pi^0$ and $K_S \to \pi^0\pi^0$ tagging samples respectively. The average result we get is 0.999 for all of the $K_{\rm cr}$ energies. This is not surprising, because we know that in 0.5% of the cases the K_L decay chain gives the wrong result for $T_0^{\rm ev}$. When correcting with the MC factor R_2 we finally get an average value of $A(\pi^0\pi^0) = 0.9999$ with systematic error of $\sim 0.4 \times 10^{-3}$. The total systematic error to the measurement of $\rm R_S^\pi$ from the evaluation of the f_n spectra and the P_n^{in}, P_n^{out} probabilities is $\sim 0.45 \times 10^{-3}$ at $E_{\rm cr} = 300\,{\rm MeV}$.

3.4 Evaluation of $\epsilon_{cr}(\pi^+\pi^-)/\epsilon_{cr}(\pi^0\pi^0)$

When computing the ratio between $\pi^+\pi^-$ and $\pi^0\pi^0$ selection efficiencies (see Eq. 1) the value of $R_K = \epsilon_{cr}(\pi^+\pi^-)/\epsilon_{cr}(\pi^0\pi^0)$ is needed, ϵ_{cr} being the MC efficiency for the $K_{\rm cr}^{\rm true}$ algorithm. The value of this ratio is shown in Fig. 11 for the three cuts on $K_{\rm cr}$ energy separately.

R_K scales with $K_{\rm cr}$ energy cut, growing from ~ 1.003 at $125\,{\rm MeV}$ up to ~ 1.008 at $300\,{\rm MeV}$. The reason for this bias cannot be the T_0, because in this case it is correctly determined from the MC truth. It is due instead to K_S daughter particles that overlap

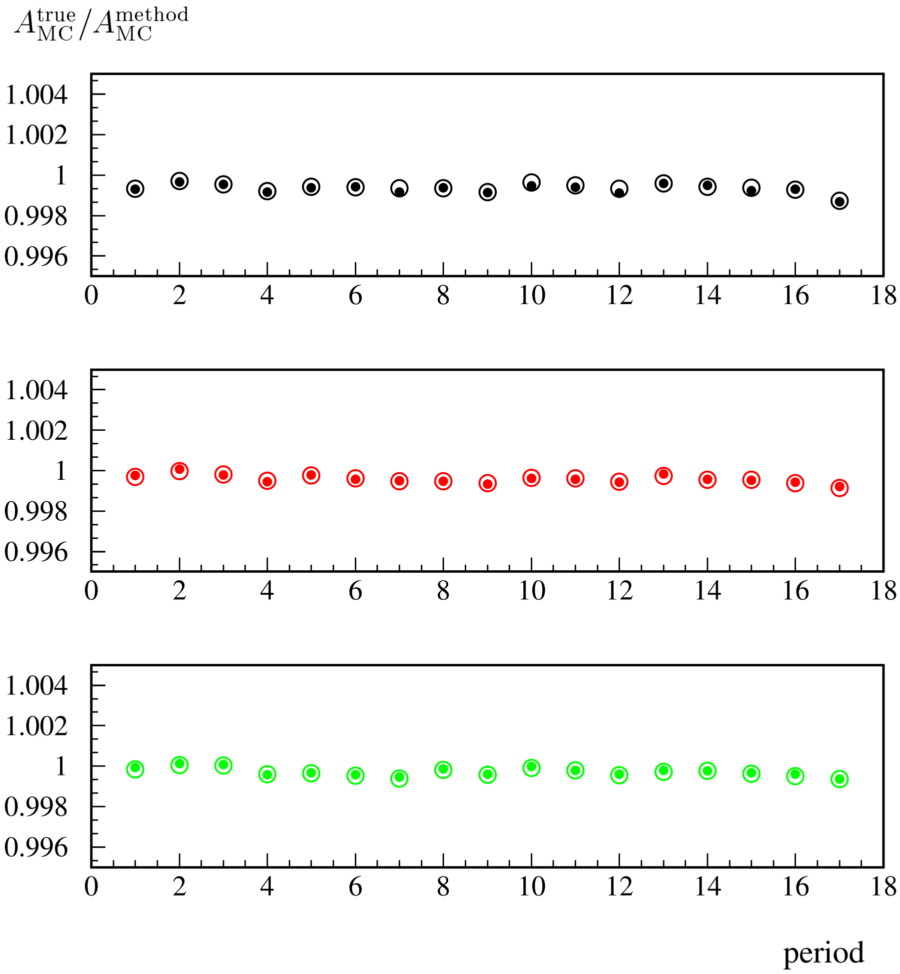

Figure 10: R_1 (full dots) and R_2 (open dots) as a function of data taking period; $E_{\rm cr} > 125\,{\rm MeV}$ (top panel), $E_{\rm cr} > 200\,{\rm MeV}$ (middle panel), $E_{\rm cr} > 300\,{\rm MeV}$ (bottom panel).

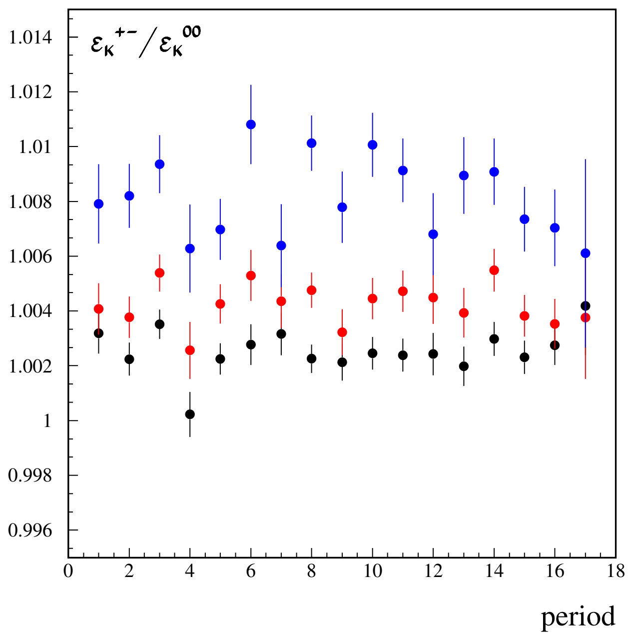

Figure 11: R_K as a function of data taking period for the three values of $E_{\rm cr}$: $E_{\rm cr} = 125\,\mathrm{MeV}$ (black), $E_{\rm cr} = 200\,\mathrm{MeV}$ (red), $E_{\rm cr} = 300\,\mathrm{MeV}$ (blue).

with K_L, then lowering its reconstruction efficiency. This is evident by looking at Fig. 12, where $\epsilon_{cr}(\pi^+\pi^-)$ and $\epsilon_{cr}(\pi^0\pi^0)$ are shown as a function of the angular distance in the transverse plane ($\Delta\phi_{\rm min}$) and the longitudinal distance (Δz) between K_L and the closest K_S decay product on the barrel. The position where particles interact in the calorimeter barrel has been evaluated for both K_S and K_L by extrapolating momenta taken from MC truth. For $\pi^+\pi^-$ events a clear drop in the efficiency occurs when pions get closer to

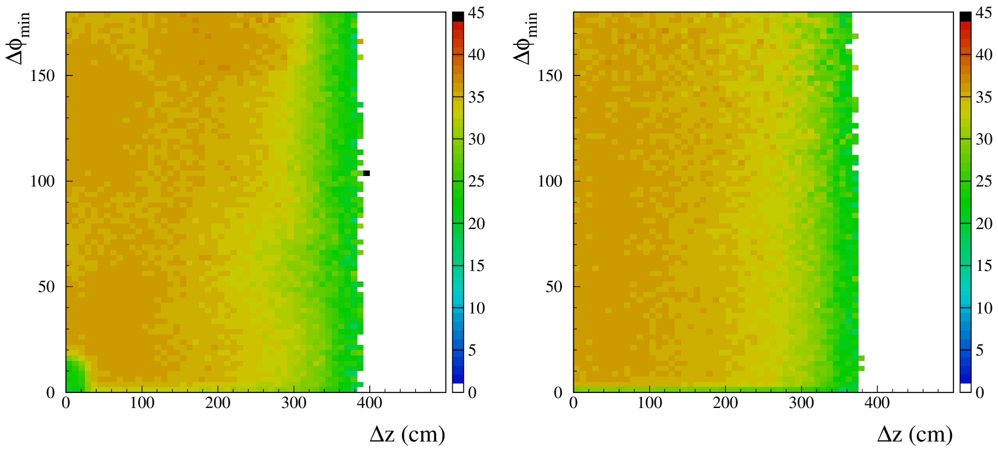

Figure 12: $\epsilon_{cr}(\pi^+\pi^-)$ (left panel) and $\epsilon_{cr}(\pi^0\pi^0)$ (right panel) as a function of $\Delta\phi_{\rm min}$ and Δz (cm); a cut $E_{\rm cr} > 125\,{\rm MeV}$ has been applied in both cases.

the K_L, because of the increasing probability of associating the K_L cluster to the pion track. For the $\pi^0\pi^0$ events we observe instead a drop at small values of $\Delta\phi_{\rm min}$, which is due to pile-up of K_S-photons and K_L in the same calorimeter cells thus giving a wrong reconstruction. The bias due to K_S-K_L overlap is not present in the rest of the plane. Indeed selecting $\pi^+\pi^-$ events with $d_{\rm min} > 100\,{\rm cm}$ ($d_{\rm min}$ is the minimum K_S-K_L distance on the barrel) and $\pi^0\pi^0$ events with $\Delta\phi_{\rm min} > 20°$ we measure $R_K = 1.0001(7)$ (period # 10).

The reliability of the MC estimate of R_K can be addressed by comparing data and MC spectra of $d_{\rm min}$ and $\Delta\phi_{\rm min}$ (Fig. 13). To estimate a systematic error on R_K we fit (see Fig. 14) with a constant the ratio between data and MC spectra in a region safe from overlap effects ($100\,{\rm cm} < d_{\rm min} < 350\,{\rm cm}$ and $\Delta\phi_{\rm min} > 25°$). This gives a normalization

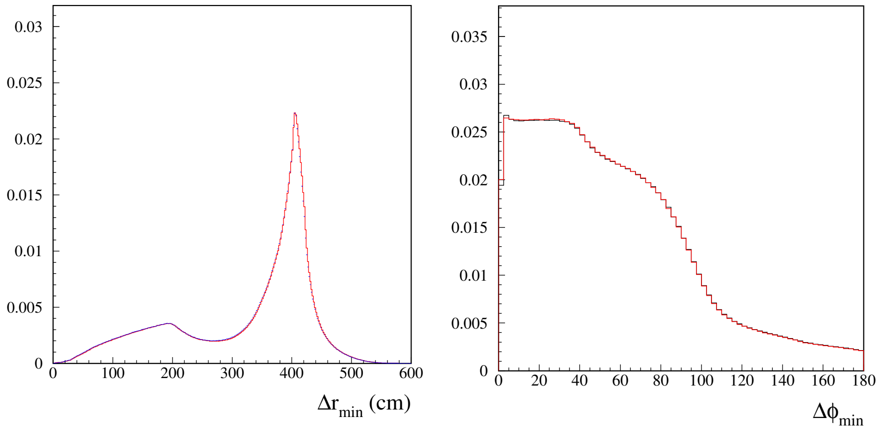

Figure 13: Left panel: data (red) and MC (blue) normalized spectra of $d_{\rm min}$ on $\pi^+\pi^-$ events; right panel: data (red) and MC (black) normalized spectra of $\Delta\phi_{\rm min}$ on $\pi^0\pi^0$ events.

factor to scale correctly the data over MC ratio in the first bins of $d_{\rm min}$ and $\Delta\phi_{\rm min}$ spectra, which are relevant to the evaluation of the overlap effect. A significant data-MC discrepancy is only present on $\pi^+\pi^-$ events when $d_{\rm min}$ goes below $10\,{\rm cm}$. Finally we correct

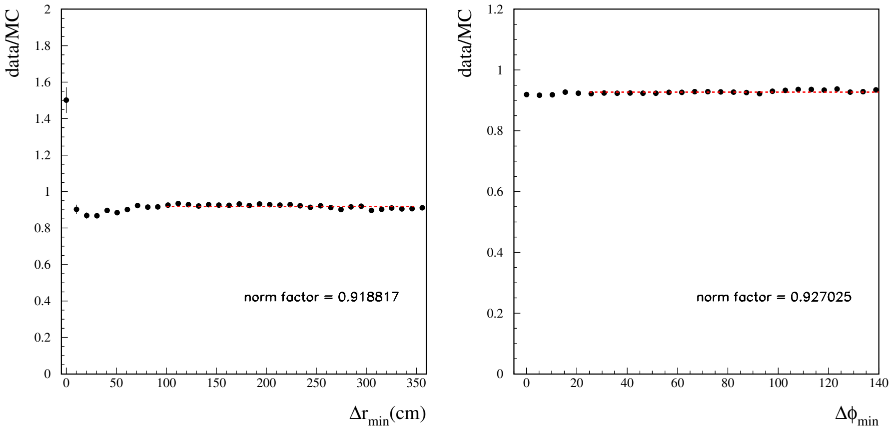

Figure 14: Left panel: data over MC ratio of $d_{\rm min}$ spectra on $\pi^+\pi^-$ events; right panel: data over MC ratio of $\Delta\phi_{\rm min}$ spectra on $\pi^0\pi^0$ events.

the MC evaluation of R_K by scaling the number of $K_{\rm cr}$ events found in the first bins of $d_{\rm min}$ and $\Delta\phi_{\rm min}$ according to the ratio we measured on data. The values of R_K before and after this correction is applied are shown in the left panel of Fig. 15 for all of the data taking periods. On the right panel we show instead the value of the correction itself. The systematic error due to the evaluation of R_K is the difference of results obtained with and without applying this correction and is $\sim 0.44 \times 10^{-3}$ for $E_{\rm cr} = 300\,{\rm MeV}$.

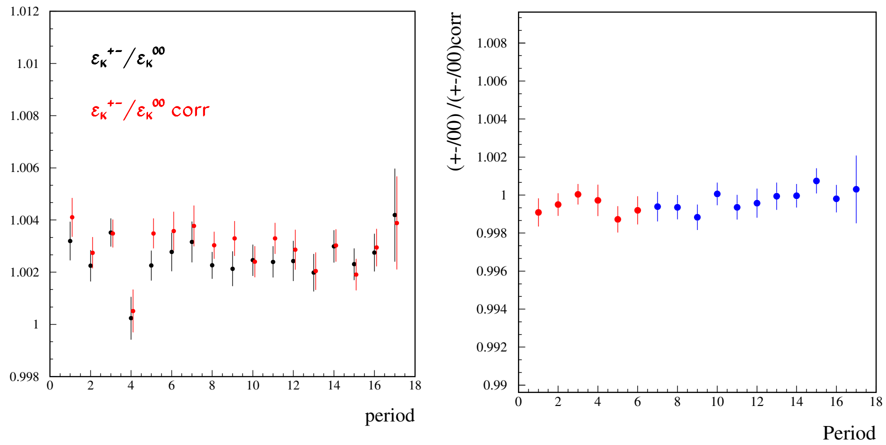

Figure 15: Left panel: R_K before (black) and after (red) the data/MC correction is applied as a function of the data taking periods; right panel: the correction to the result as a function of the data taking period.

4 $K_S \to \pi^0\pi^0$: signal selection and acceptance evaluation

Starting from the sample of $K_{\rm cr}$ tagged events, $K_S \to \pi^0\pi^0$ decays are identified by the prompt photon clusters from the π^0 decays. A prompt photon cluster must satisfy $|t_{\rm cl} - r_{\rm cl}/c| \leq \min(5\sigma_t, 3\,{\rm ns})$, where σ_t is the energy-dependent time resolution, and must not be associated to any track. Machine background is reduced by cuts on energy and polar angle; we require $E_{\rm cl} > 20\,{\rm MeV}$ and $\cos\theta_{\rm cl} < 0.9$. Three or more prompt photons are required to accept a $K_S \to \pi^0\pi^0$ event. Further cuts have been implemented to enhance the rejection power on a particular topology of machine background events ("splash events"); these will be discussed in Sec. 4.5.

The acceptance is evaluated by using MC. The multiplicity spectrum we observe on a sample of simulated $\pi^0\pi^0$ events (given a $K_{\rm cr}$ tag) is composed by 2% 1-prompt, 8% 2-prompt, 35% 3-prompt and 55% ≥ 4-prompt events. It can be systematically shifted by one of the following reasons:

- A discrepancy between data and MC in the cluster reconstruction efficiency ($\epsilon_{\rm cl}(\rm data) \neq \epsilon_{\rm cl}(\rm MC)$).
- A discrepancy between data and MC in the amount of split clusters ($\rm P_{\rm split}(\rm data) \neq \rm P_{\rm split}(\rm MC)$) and of photon conversions.
- A wrong amount of accidental clusters from machine background inserted in the simulation. This affects the probability for an accidental hit arriving early in time to "steal" the $T_0^{\rm ev}$ to K_S photons, thus causing the event loss. Moreover a displacement can be produced in the probability for an accidental cluster itself to enter the prompt cluster selection ($\rm P_{\rm acci}(\rm data) \neq \rm P_{\rm acci}(\rm MC)$) thus affecting the multiplicity counting.
- A discrepancy between data and MC in the amount of event losses due to a wrong $T_0^{\rm ev}$ evaluation from K_S photons themselves, when clusters are merged together or in presence of other instrumental effects.

All of these effects have been accounted for in the final acceptance computation, as will be discussed in the following subsections.

4.1 Effect of photon detection efficiency

The photon detection efficiency is measured on samples of $\phi \to \pi^+\pi^-\pi^0$ events. These are selected by the following analysis steps:

- Two tracks from IP with opposite charge are required; the missing four-momentum is calculated in the $\phi \to \pi^+\pi^-\pi^0$ hypothesis: $p_{\pi^0} = p_\phi - p_{\pi^+} - p_{\pi^-}$; the missing mass is selected in a $x - \sigma$ range around the π^0 mass.
- A photon from π^0 decay is selected as a *tagging* photon (γ_1), by cutting around the expected time and energy; the latter is derived from the π^0 momentum and the cluster position by imposing the two-body π^0 decay: $\mathrm{E}_\gamma = m^2_{\pi^0}/2(E_{\pi^0} - p_{\pi^0}\cos\theta_{\pi^0\gamma_1})$.
- To perform an unbiased search, the calorimeter trigger requests have to be fulfilled by the charged pions and the *tagging* photon alone.
- A *matching* cone is defined with $\cos\theta > 0.8$ around the expected line of flight of the second photon ($\mathrm{p}_{\gamma_2} = \mathrm{p}_{\pi^0} - \mathrm{p}_{\gamma_1}$). A separation cut requires the charged pions and the *tagging* photon to be outside of the *matching* cone.
- Dedicated cuts are applied to reject the residual $e^+e^-\gamma$ background ($\sim 3\%$); these comprehend the time of flight of the clusters associated to the tracks (pion hypothesis), their depth and the E/p ratio, the polar angle between the charged tracks.

The efficiency is evaluated by counting the events with a photon *matching* the cone around the expected direction. Photon counting is performed in bins of the polar angle (θ_γ) and of the expected energy (E_γ). What is relevant for our purpouse is the ratio between the efficiency observed on data and MC events. Fig. 16 shows such a ratio as a function of E_γ for two different polar angle regions: $85^\circ < \theta_\gamma < 90^\circ$ on the left panel, $30^\circ < \theta_\gamma < 35^\circ$ on the right panel. The need is evident for a correction in the low energy region, especially when going in the angular region covered by calorimeter endcaps. The present analysis result (black dots) has been fitted (black curve) with a three parameter function

$$\epsilon_{\mathrm{cl}}(\mathrm{data})/\epsilon_{\mathrm{cl}}(\mathrm{MC}) = \mathrm{K}\int_{-\infty}^{(-\mathrm{E}_\gamma-\mu)/\sigma} Gauss(x)dx,$$

giving the plateau, the centre and the width of the correction. The blue curve represents the correction profile we used for 2000 data. The red curve represents what we would get by letting in the data sample the radiative Bhabha contamination. Fig. 17 shows the

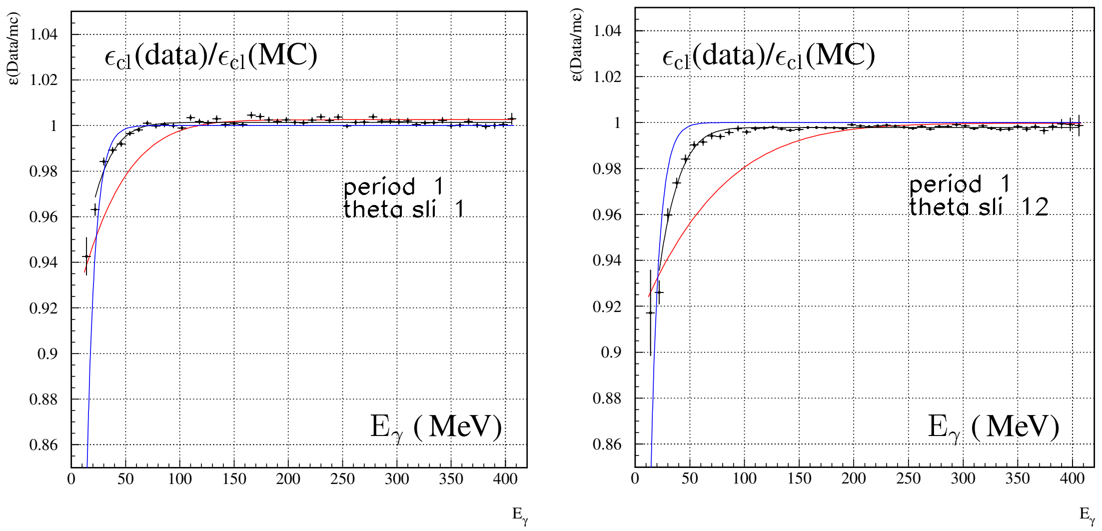

Figure 16: ϵ_{cl}(data)/ϵ_{cl}(MC) as a function of E_γ for two polar angle regions: $85° < \theta_\gamma < 90°$ on the left panel, $30° < \theta_\gamma < 35°$ on the right panel.

fit results for all of the 17 periods of 2001-2002 data sample for $40° < \theta_\gamma < 45°$. Red dots represent the 2001 and 2002 average results respectively. The ratio between data and MC photon efficiencies is used when evaluating $\pi^0\pi^0$ selection efficiency with MC. The correction is implemented by switching off MC clusters with random extraction according to the efficiency ratio profile, in the appropriate polar angle and energy bin. Fig. 18 shows the ratio between the corrected and uncorrected MC acceptance as a function of data taking period. The systematic shift is 3-4 per-mil on average, with 1 per-mil fluctuations as a function of run period. To test the validity of the applied correction we checked the reliability of MC in reproducing the observed prompt multiplicities (given a K_{cr} tag). The multiplicity spectrum is influenced by other effects too, e.g. splitting or accidental contamination, but these are suppressed when cutting at $E_\gamma > 20\,\mathrm{MeV}$ (see Sec. 4.2). Because of background affecting 1-prompt and 2-prompt events we compare data and

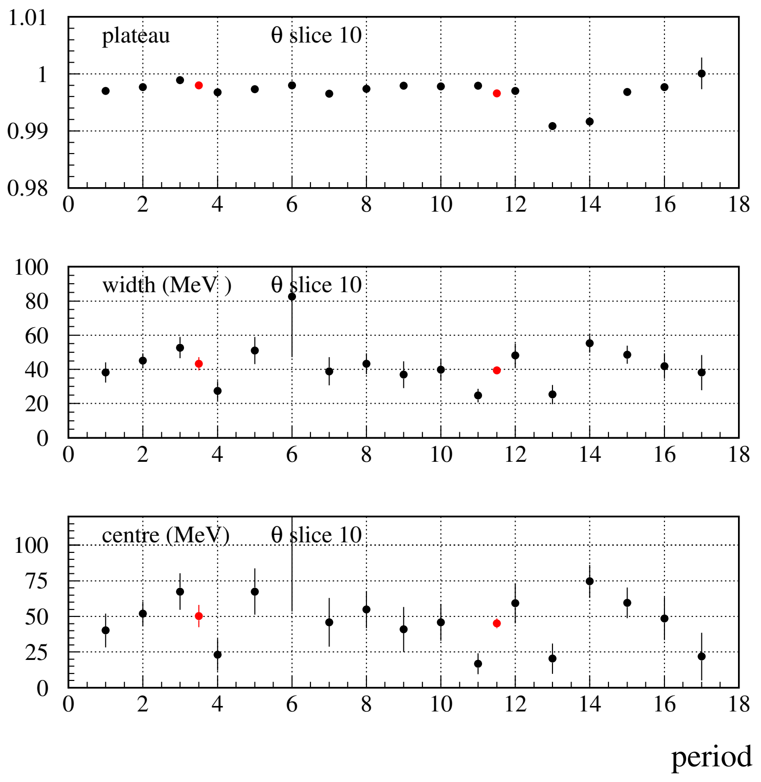

Figure 17: ϵ_{cl}(data)/ϵ_{cl}(MC) fit results for 2001-2002 dataset; red dots represent 2001 and 2002 average results respectively.

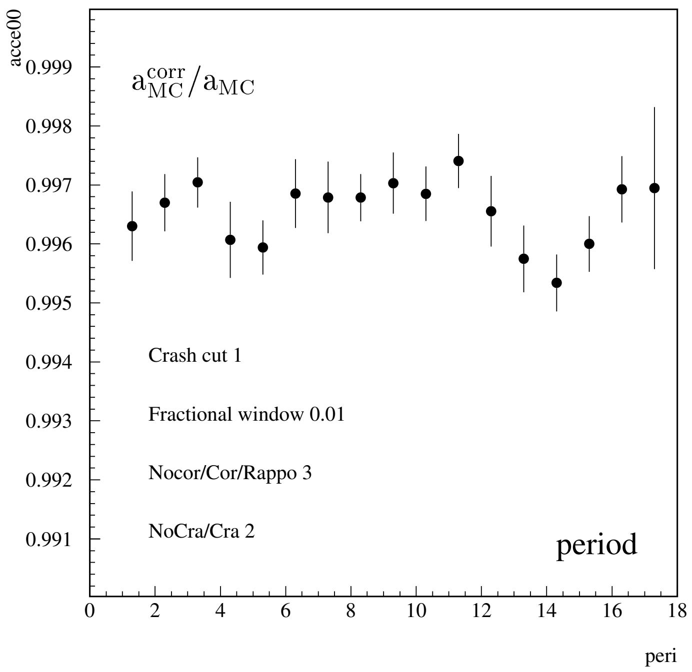

Figure 18: Relative effect of data over MC cluster efficiency correction on $\pi^0\pi^0$ acceptance, as a function of data taking period.

MC by normalizing counts to the integral of events with more than 2 prompt clusters. In Fig. 19 such a comparison is shown for 3-prompt ($N_3/N_{\geq 3}$) and 4-prompt ($N_4/N_{\geq 3}$) events. MC points are shown before (open red dots) and after (blue triangles) the cluster efficiency correction is applied. Agreement between data and MC is better than 1%. Robustness of the cluster counting is checked by varying the cut on the prompt cluster

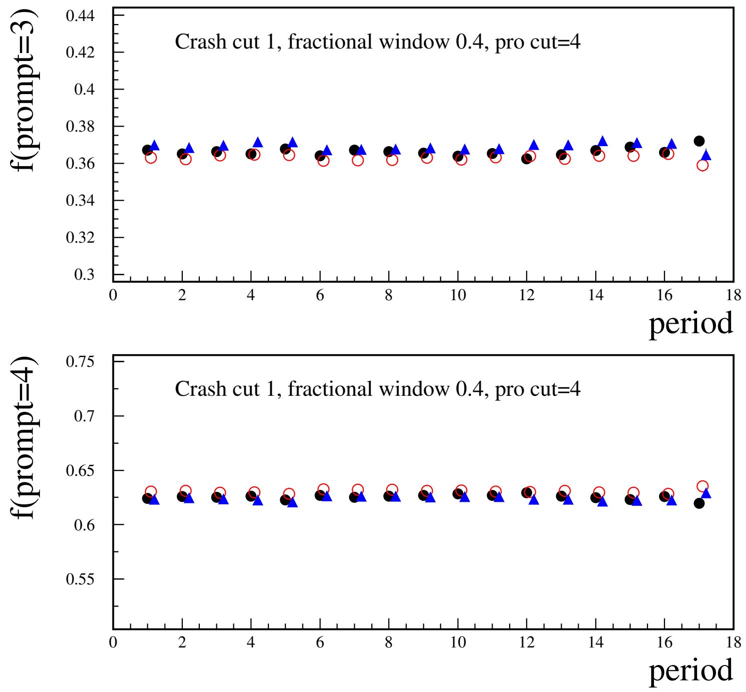

Figure 19: ($N_3/N_{\geq 3}$ (upper panel) and $N_4/N_{\geq 3}$ (lower panel) as a function of data taking for data (black), MC (open red) and MC corrected by $\epsilon_{\rm cl}$(data)/$\epsilon_{\rm cl}$(MC).

energy between 7 MeV and 50 MeV (standard cut is 20 MeV). In Fig. 20 we show the ratio $(N_3/N_{\geq 3})_{\rm data}/(N_3/N_{\geq 3})_{\rm MC}$ as a function of the cut on E_γ for all the periods of 2001 data taking. As a result of the cluster efficiency correction we get a data-MC agreement which is remarkably good down to 7 MeV. Residual effects can be abscribed to splitting and accidental contamination.

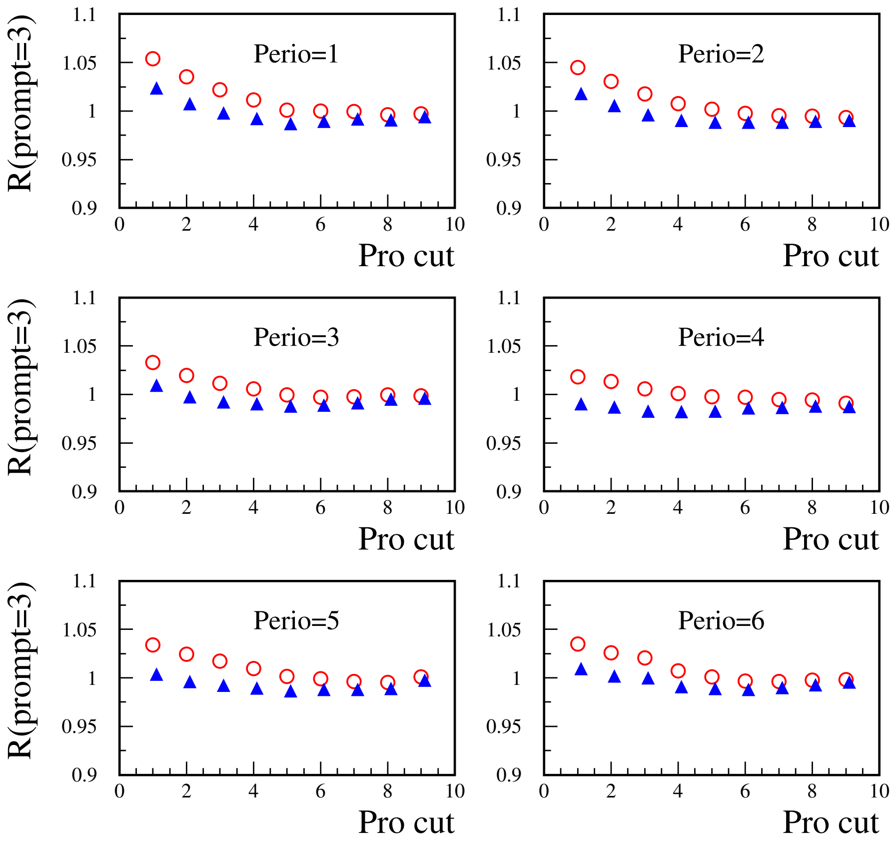

Figure 20: $(N_3/N_{\geq 3})_{\mathrm{data}}/(N_3/N_{\geq 3})_{\mathrm{MC}}$ as function of E_γ cut for 2001 data taking.; MC is shown before (open red) and after (blue) the cluster efficiency correction; cut legenda: 1=7 MeV, 2=10 MeV, 3=15 MeV, **4=20** MeV **(standard)**, 5=25 MeV, 6=30 MeV, 7=35 MeV, 8=40 MeV, 9=50 MeV.

To assign a systematic uncertainty to the acceptance we check the stability of the estimated $\pi^0\pi^0$ signal events as a function of the cut on the prompt cluster energy. We evaluate the ratio

$$R_{syst} = \frac{N_{\geq 3}/a\,[\mathrm{E}_\gamma > \mathrm{E_i}]}{N_{\geq 3}/a\,[\mathrm{E}_\gamma > 20\,\mathrm{MeV}]},$$

where $N_{\geq 3}$ is the number of selected $\pi^0\pi^0$ events on data and a is the MC acceptance for each value of E_γ cut. This ratio R_{syst} is very stable and close to one, as it is shown in Fig. 21 for six periods of 2002 data sample. In the same E_γ cut interval the acceptance goes from $a(\mathrm{E}_\gamma > 7\,\mathrm{MeV}) = 0.920$ to $a(\mathrm{E}_\gamma > 50\,\mathrm{MeV}) = 0.735$. The final systematic uncertainty is evaluated by taking the rms variation of R_{syst} for each period and making the average between all of the periods. The rms values are shown as a function of the data taking period in Fig. 22. The systematic error on the cluster counting is $\sim 0.50 \times 10^{-3}$ for $E_{\mathrm{cr}} = 300\,\mathrm{MeV}$.

4.2 Effect of split and accidental clusters

Accidental clusters from machine background which arrive early respect to the collision time are able to "steal" the T_0^{ev} to K_S photons in 1-2% of the cases. This produces a corresponding loss of events. Background hits are taken from real $\gamma\gamma$ events and inserted into the simulated events proportionally to the observed background rate. A bug in the insertion code enhanced the rate of accidental clusters. This error amounts to a factor of ~ 2 in the 2002 data sample. Matteo Martini and Stefano Miscetti evaluated a set of constants [8] to downscale the accidental clusters to the appropriate level. In Fig. 23 the ratio is shown between the acceptance after the correction to accidentals is applied and the previously calculated value. The effect is particularly visible on 2002 sample, where the old MC version underestimated the acceptance by as much as 0.8%. Given the size of the correction it is of great importance to cross-check independently the agreement between data and MC on the rate of accidentals. This is obtained by measuring the probability of having an accidental entering the prompt cluster selection. Events with 5 prompt clusters (given a K_{cr}) are used to this purpouse, which have *always* either an accidental or a split cluster. The pair of clusters with minimum distance (d_{min}) is selected. The population of split clusters peaks at small values of d_{min}. This is clearly visible as a peak in the plane

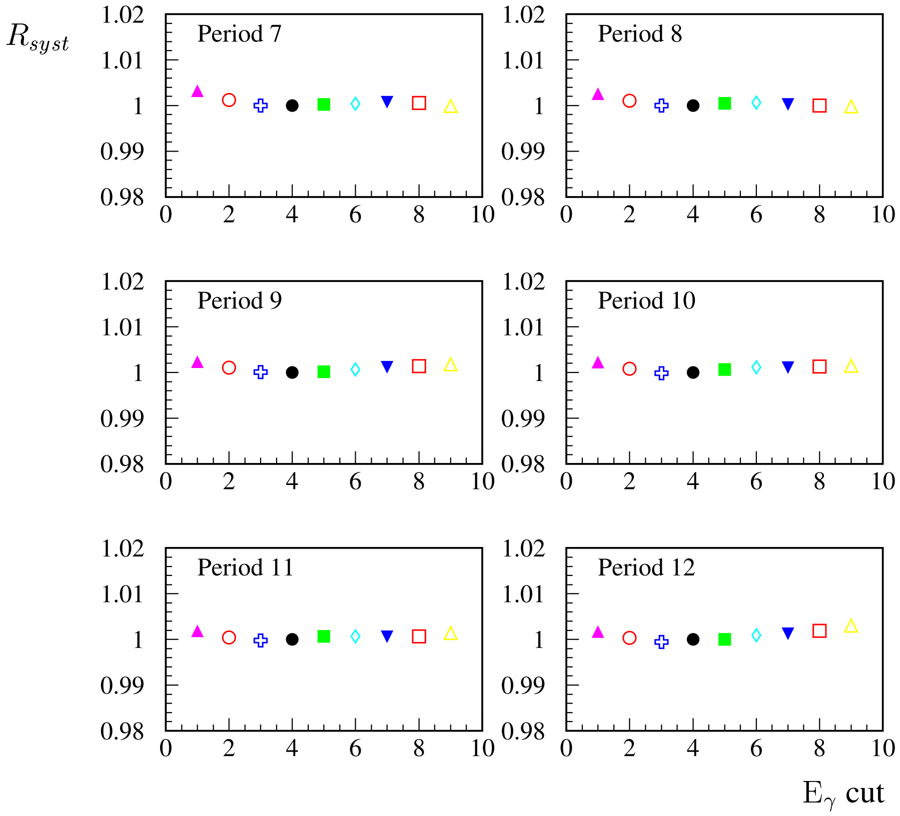

Figure 21: R_{syst} plotted as a function of E$_\gamma$ cut for six periods belonging to 2002 data taking; cut legenda: 1=7 MeV, 2=10 MeV, 3=15 MeV, **4=20** MeV **(standard)**, 5=25 MeV, 6=30 MeV, 7=35 MeV, 8=40 MeV, 9=50 MeV.

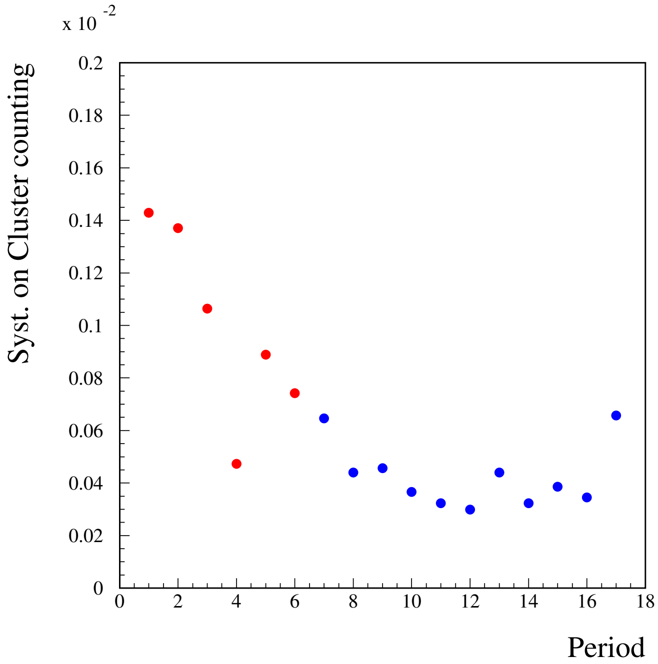

Figure 22: Rms value of R_{syst} as a function of data taking period.

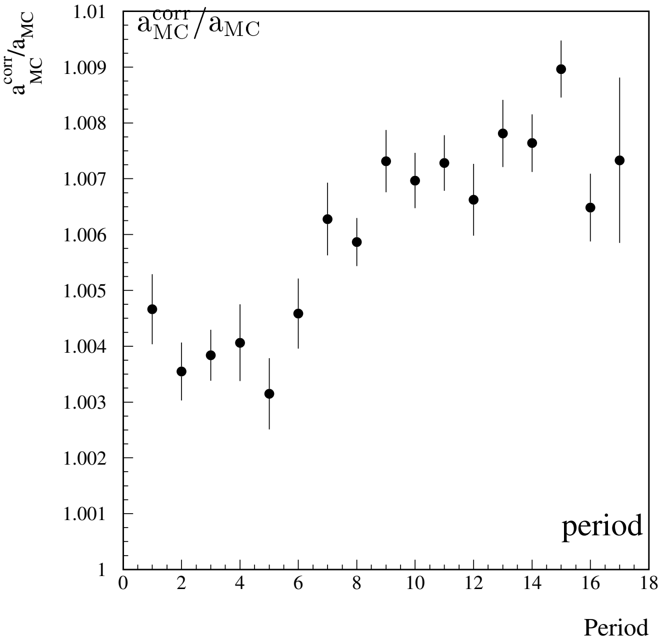

Figure 23: Ratio between the acceptance before and after the correction on background clusters has been applied.

of the minimum energy between the coupled clusters versus $d_{\min}$ (see Fig. 24). Cutting at

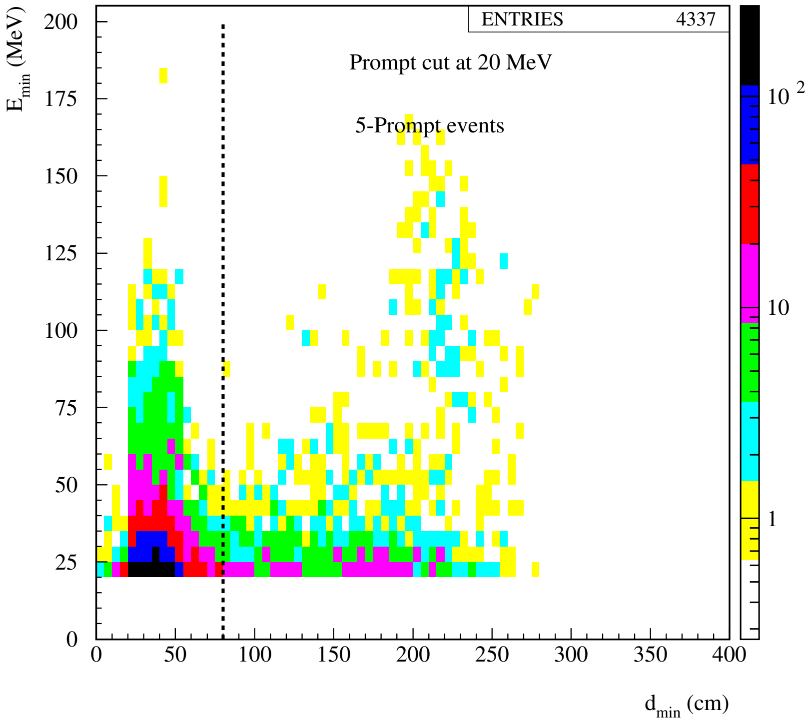

Figure 24: Scatter plot of minimum energy versus distance for the couple of closest clusters in 5-prompt events.

$d_{\min} < 80\,\mathrm{cm}$ it is possible to count separately the events with split clusters (N_{split}) and those with accidental clusters (N_{acci}). Then we get the splitting and accidental probability from:

$$P_{\mathrm{split}} = N_{\mathrm{split}}/(4N_4) \qquad\qquad P_{\mathrm{acci}} = N_{\mathrm{acci}}/N_4,$$

where N_4 is the number of 4-prompt events in the same sample. P_{split} and P_{acci} have been calculated on both data and MC, and they are shown as a function of data taking period in Fig. 25 (left and right panel, respectively). The data points (black) for P_{split} are shifted upward by 10^{-3} respect to the MC ones (open red). The corresponding correction induced on the acceptance is equal to $(P^{\mathrm{data}}_{\mathrm{split}} - P^{\mathrm{MC}}_{\mathrm{split}}) \times N_2/N_{\geq 3} \sim 10^{-4}$, where the prompt multiplicities are taken from MC signal. This correction is shown in the left panel of Fig. 26 as a function data period. The difference between corrected and uncorrected final results is taken as a systematic error, and is 0.11×10^{-3} independent of $E_{\rm cr}$.

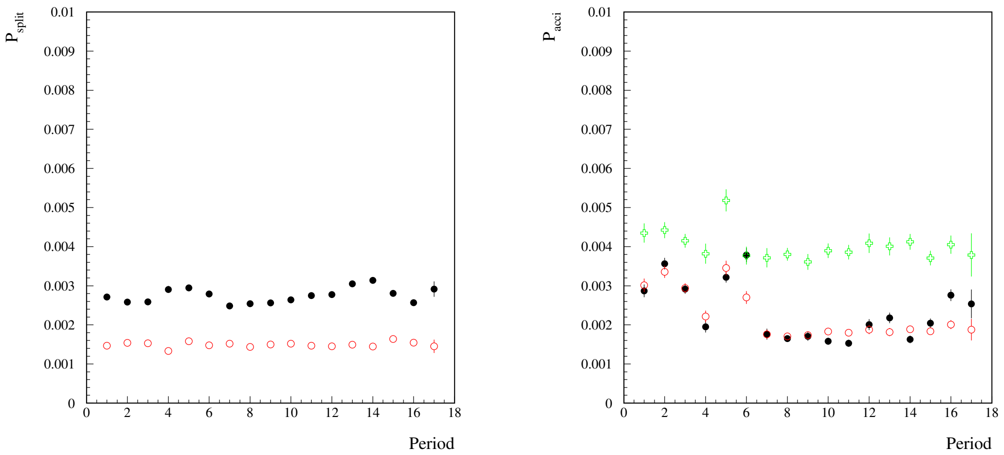

Figure 25: $P_{\rm split}$ (left panel) and $P_{\rm acci}$ (right panel) for data (black) and MC (open red); green dots in the left panel are from MC with the wrong background content.

Turning now to $P_{\rm acci}$, in the lower panel data point (black) are compared with MC before (green) and after (open red) the error on the background content has been removed. The fractional correction to the acceptance coming from the observed data-MC difference in the accidental rate is evaluated for each period through the equation:

$$1 - \frac{P^{\rm data}_{\rm acci} - P^{\rm MCcorr}_{\rm acci}}{P^{\rm MC}_{\rm acci} - P^{\rm MCcorr}_{\rm acci}} \times (\frac{a_{\rm MCcorr}}{a_{\rm MC}} - 1).$$

This correction is sizeable for period #6 and for the last 3 periods of 2002, for which the calibration factors have larger uncertainty. However, since the systematic uncertainty in the rate of accidental cluster also affects in a similar way the $\pi^+\pi^-$ selection efficiency, we will show in Sec. 5.3 that a cancellation occurs between the two corrections. The final systematic error induced will be discussed at the end of Sec. 5.3.

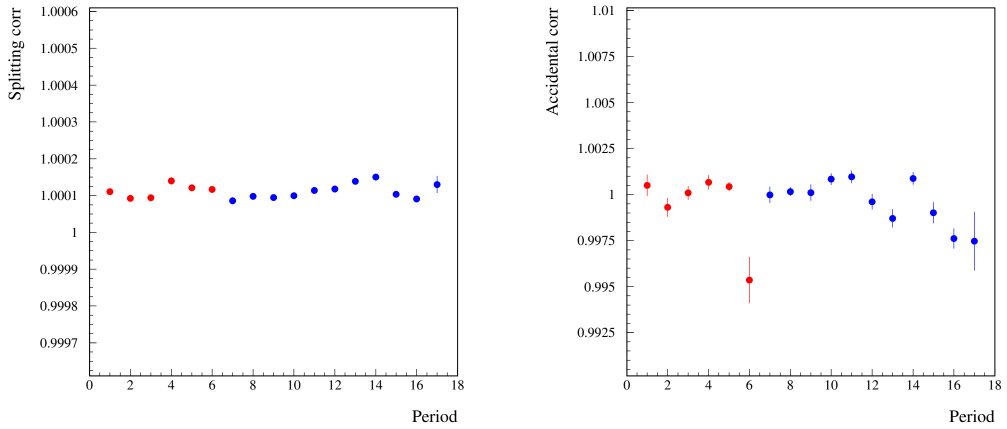

Figure 26: Corrections to the $\pi^0\pi^0$ acceptance due to the difference between data and MC splitting probabilities (left panel) and to the uncertainty in the calibration of the rate of accidental clusters in the MC (right panel).

4.3 Effect of photon conversions

Photons from π^0 decays have $\sim 1.5 \times 10^{-3}$ probability to convert into an e^+e^- pair by interacting before entering the DC volume. These events ($\sim 6 \times 10^{-3}$ of the total) produce at maximum three prompt clusters, therefore they are selected with a lower efficiency: $a_{\text{couple}} \sim 0.67$ instead of $a \sim 0.89$. The $\pi^0\pi^0$ acceptance a_{av} is computed on MC by averaging a_{couple} and a with weights equal to f_{couple} and $1. - f_{\text{couple}}$ respectively, where f_{couple} is the probability for at least one of the photons from π^0 decay to interact in the beam pipe or in the DC inner walls and to produce an e^+e^- pair. The systematic uncertainty on a_{av} is related essentially to the amount of material which is inserted in the simulation of the apparatus.

In order to test the MC reliability in reproducing the correct amount of photon conversions, we exploit a peculiar characteristic of these events, that is the presence of a couple of tracks from the IP. From MC we measure indeed a probability $p_{\text{trk}}^{\text{MC}} \sim 0.74$ to observe at least one track from IP after the $\pi^0\pi^0$ selection has been applied. This is possible because our $\pi^0\pi^0$ selection does not apply any track veto. The events with a Dalitz π^0 decay (~ 0.024 of the total) have exactly the same topology of those with photon conversion, but give a negligible contribution to the systematic uncertainty.

In Fig.27 the fraction of events with at least one track from IP is shown for data ($f_{\rm trk}^{\rm data}$), MC events ($\phi \to all$ sample) selected as in data ($f_{\rm trk}^{\rm MC}$), and $\pi^0\pi^0$ decays selected from MC truth ($f_{\rm trk}^{\rm MCtrue}$). Two thirds of the events with tracks from the IP are due to Dalitz π^0 decays, while the rest come from photon conversions. A small discrepancy ($< 10^{-3}$) is observed between MC $\phi \to all$ and truly $K_S \to \pi^0\pi^0$ decays, which is due to the residual K^+K^- background contamination (see Sec.9), which is still present when selecting events with $E_{\rm cr} = 300\,{\rm MeV}$.

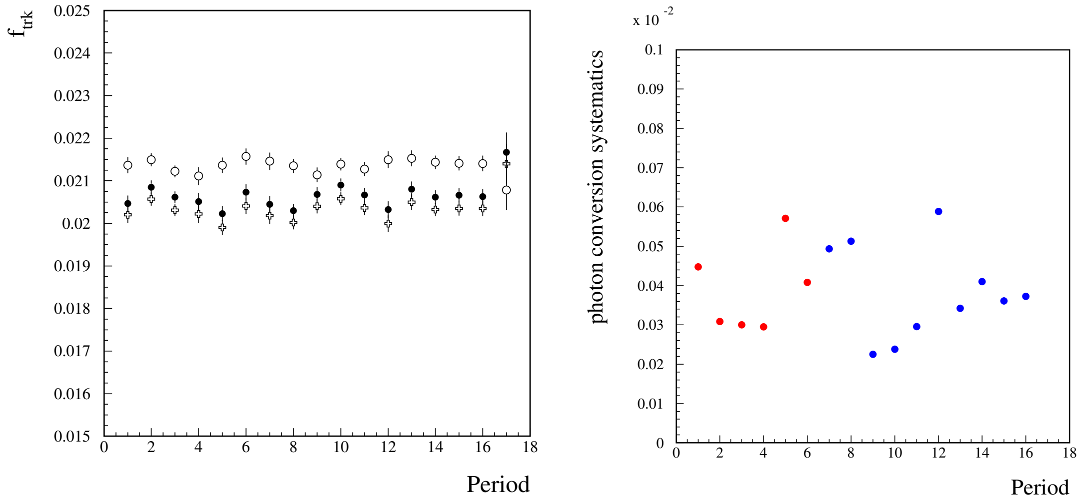

Figure 27: Left panel: $f_{\rm trk}^{\rm data}$ (open dots), $f_{\rm trk}^{\rm MC}$ (filled dots) and $f_{\rm trk}^{\rm MCtrue}$ (open crosses) as a function of the data taking period; right panel: fractional systematic error induced on the $\pi^0\pi^0$ acceptance by photon conversion simulation, as a function of the data taking period.

The difference $f_{\rm trk}^{\rm data} - f_{\rm trk}^{\rm MC}$ is instead $\sim 10^{-3}$, and it can be abscribed to some data-MC difference in the photon conversion cross section. This difference induces a systematic shift in the $\pi^0\pi^0$ acceptance, which is be evaluated as follows:

$$\frac{\Delta a}{a} = \frac{f_{\rm trk}^{\rm data} - f_{\rm trk}^{\rm MC}}{p_{\rm trk}^{\rm MC} a_{\rm couple}} \times \frac{a - a_{\rm couple}}{a},$$

where the first term represents the difference between the number of data and MC photon conversion events, and the second term is the fractional loss of efficiency which is induced by photon conversion. The value of $\Delta a/a$ is shown in the right panel of Fig.27 as a function of the data taking period; the average over the periods is 0.38×10^{-3}, independent of $E_{\rm cr}$.

4.4 Probability for a wrong $T_0^{\rm ev}$ from K_S photons

Being the prompt cluster search very sensitive to the $T_0^{\rm ev}$ determination, we have investigated also other possible sources for a wrong $T_0^{\rm ev}$ reconstruction. To perform this study we selected a sample of $K_S \to \pi^0\pi^0$ events given a $K_L \to \pi^+\pi^-\pi^0$ tagging decay. In this case we can select prompt photons by using an independent determination of the T_0 from the K_L decay chain, $T_0(K_L)$. On these events the difference (ΔT_0) is calculated between $T_0^{\rm ev}$ and $T_0(K_L)$, the latter being always true. The spectrum of $\Delta_{\rm bunch} = \Delta T_0/T_{\rm RF}$ is shown in the left panel of Fig. 28. The negative tail with $\Delta_{\rm bunch} \leq -4$ is dominated by machine background clusters. A clear step is evident in the range $-3 \leq \Delta_{\rm bunch} \leq -1$, for which other effects start to play a role.

- First is cluster merging of two K_S photons close in ϕ on the calorimeter barrel. This effect, which has been investigated by looking at the MC truth, is responsible for a maximum time shift of 3 bunches, corresponding to half of the module length approximately.

- Second is the presence of hot ADC channels which can unbalance the average between calorimeter sides, thus giving a wrong time reconstruction. This is confirmed by looking at Fig. 29, where the transverse position of the cluster producing the $T_0^{\rm ev}$ is shown for data an MC separately (barrel case). Spectra are filled with the condition $-3 \leq \Delta_{\rm bunch} \leq -1$. On real data a clear peak appears, showing an instrumental effect which is indeed absent for MC events. Such an effect obviously depends on the run period.

Therefore the integral of events with $-3 \leq \Delta_{\rm bunch} \leq -1$ normalized to the total number of entries gives the probability of having a wrong $T_0^{\rm ev}$ from K_S or residual accidentals

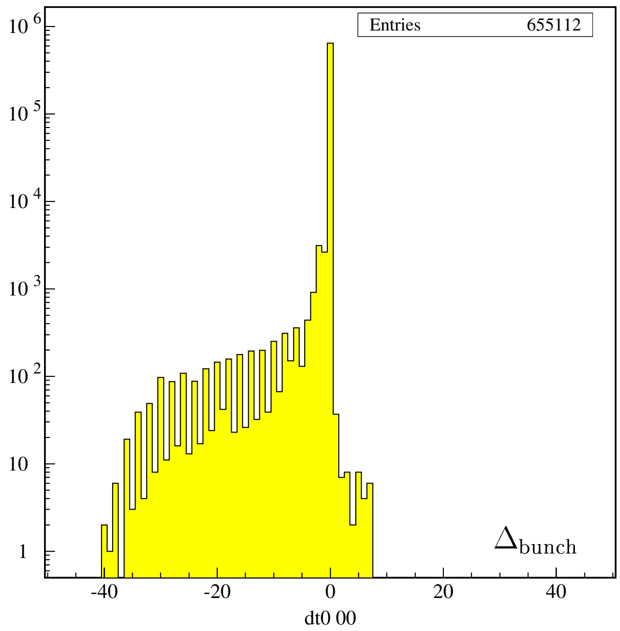

Figure 28: Δ_{bunch} spectrum for $K_S \to \pi^0\pi^0$, $K_L \to \pi^+\pi^-\pi^0$ events.

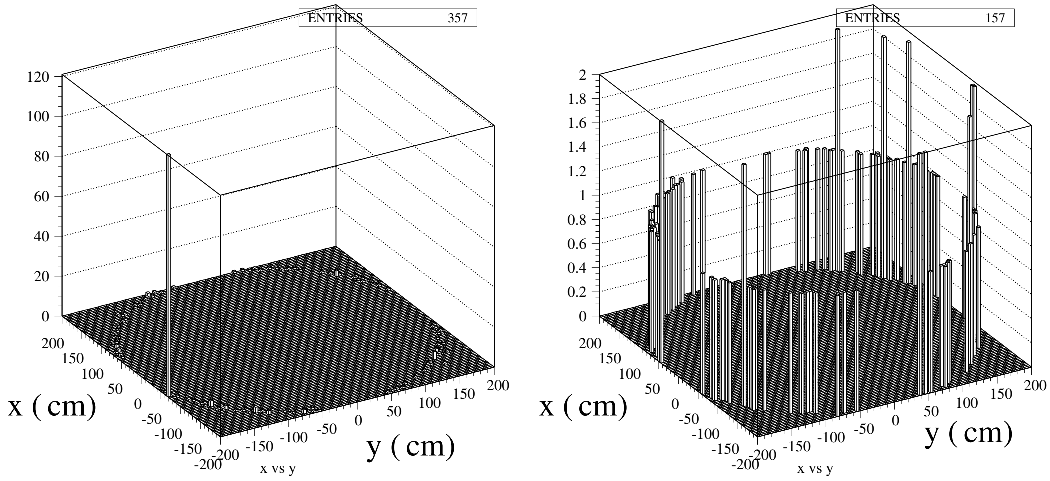

Figure 29: Transverse position for T_0^{ev} cluster on the barrel, selected with $-3 \leq \Delta_{\mathrm{bunch}} \leq -1$; data on the left panel, MC on the right one.

for data ($P^{\mathrm{data}}_{\mathrm{autorubo}}$) and MC ($P^{\mathrm{MC}}_{\mathrm{autorubo}}$). The acceptance is then scaled by $C_{\mathrm{autorubo}} = 1 - P^{\mathrm{data}}_{\mathrm{autorubo}} + P^{\mathrm{MC}}_{\mathrm{autorubo}}$. On the left panel of Fig. 30 the values of $P^{\mathrm{data}}_{\mathrm{autorubo}}$ (black dots) and $P^{\mathrm{MC}}_{\mathrm{autorubo}}$ (red dots) are shown for all the data taking periods. Refer to the left axis for the vertical scale. The correction is shown in the same plot (blue, vertical axis on the right) and spans between 0.992 and 0.999.

The systematic uncertainty related to this correction is estimated on MC. We compare the number of photon merging we find on selected $K_S \to \pi^0\pi^0$- $K_L \to \pi^+\pi^-\pi^0$ events with the number of wrong T_0 from K_S (from MC truth) we get on $K_S \to \pi^0\pi^0 K_{\mathrm{cr}}$ events. These two quantities are shown in the right panel of Fig. 30 as a function of data taking period. A 0.6×10^{-3} systematic error is evaluated for this correction.

4.5 Machine background contamination

Particularly during 2001 the event selection was affected by machine background events capable to satisfy K_{cr} tag while giving at the same time 3 prompt clusters (“splash events”,

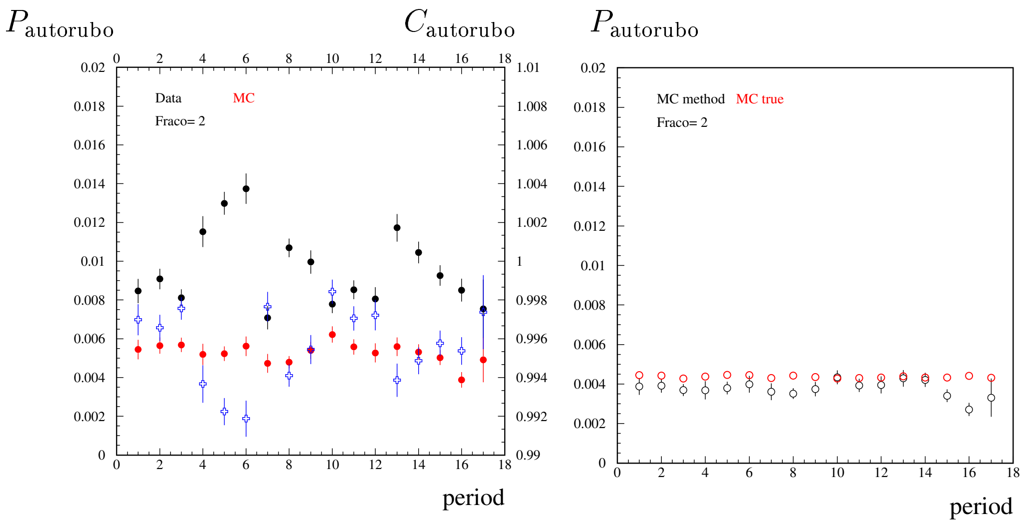

Figure 30: Left panel: $P^{\rm data}_{\rm autorubo}$ (black), $P^{\rm MC}_{\rm autorubo}$ (red) and $C_{\rm autorubo}$ (blue) as a function of the run period; right panel: comparison on MC events between method (open black) and MC truth (open red) on the probability of wrong T_0 from K_S.

for a detailed study see [9]). The background contamination is particularly evident when lowering the cut on E_γ. In Fig. 31 the scatter plot of average transverse position ($\rho_{av} = \sum_i \rho_i E_i$) versus average energy E_{av} of 3-prompt cluster events is shown. The selection is repeated with $\mathrm{E}_\gamma > 7\,\mathrm{MeV}$ and $\mathrm{E}_\gamma > 20\,\mathrm{MeV}$. The spurious contribution from splash events is visible at small values of ρ_{av} and E_{av}. A series of cuts have been defined to achieve an optimal background rejection, which are reported in Tab. 4. The effectiveness

cut 1	no cut
cut 2	$\rho_{av} > 150\,\mathrm{cm}$ .OR. $E_{av} > 50\,\mathrm{MeV}$
cut 3	$\rho_{av} > 170\,\mathrm{cm}$ .OR. $E_{av} > 60\,\mathrm{MeV}$
cut 4	$\rho_{av} > 185\,\mathrm{cm}$ .OR. $E_{av} > 60\,\mathrm{MeV}$
cut 5	$\rho_{av} > 200\,\mathrm{cm}$ .OR. $E_{av} > 60\,\mathrm{MeV}$

Table 4: Definition of cuts for “splash events” rejection.

of this strategy is checked by comparing data and MC prompt normalized multiplicities

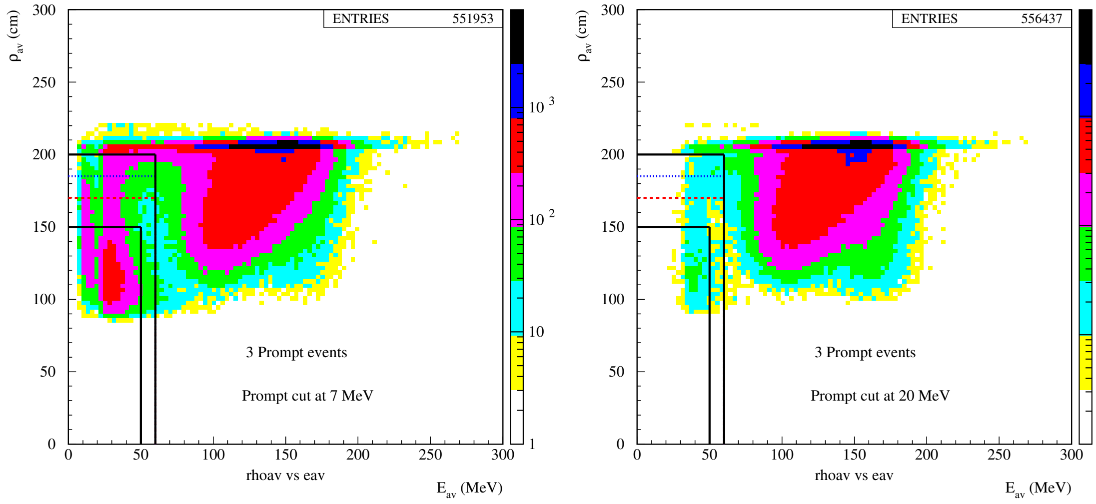

Figure 31: (ρ_{av} vs E_{av} for 3-prompt events; $\mathrm{E}_\gamma > 7\,\mathrm{MeV}$ on the left panel, $\mathrm{E}_\gamma > 20\,\mathrm{MeV}$ on the right.

before and after the application of cut 5 (Fig. 32). Here events selected with $\mathrm{E}_\gamma > 7\,\mathrm{MeV}$ are considered, which have the maximum background contamination.

The standard cut for our analysis is # 4, which has an acceptance for signal (selected with $\mathrm{E}_\gamma > 20\,\mathrm{MeV}$) of 0.99956(1) (2002 average). The background contamination before cuts is studied by evaluating the quantity $Q_i = \frac{N_1/\epsilon_1}{N_i/\epsilon_i}$, where N_i and ϵ_i are the number of selected events and the MC efficiency at cut i respectively. In the limit of no background contamination at cut i this quantity corresponds to $1 + B_1/S$ (we neglect signal efficiency variations with splash cut), where B_1 is the background content without cuts. The behaviour of Q as a function of splash cut is shown in Fig. 33 for two periods belonging to 2001 and 2002 data taking respectively. Different colours correspond to different cut on E_γ. With $\mathrm{E}_\gamma > 20\,\mathrm{MeV}$ (black points) we observe that already at cut 5 a plateau has been reached; *i.e.* no residual background at cut 5 is assumed. The initial background contamination is therefore $2-3\times10^{-3}$ and below 10^{-3} for 2002. The residual contamination at the chosen working point (cut 4) is

$$B_4/S = 1 - \frac{N_5}{\epsilon_5} \times \frac{\epsilon_4}{N_4}.$$

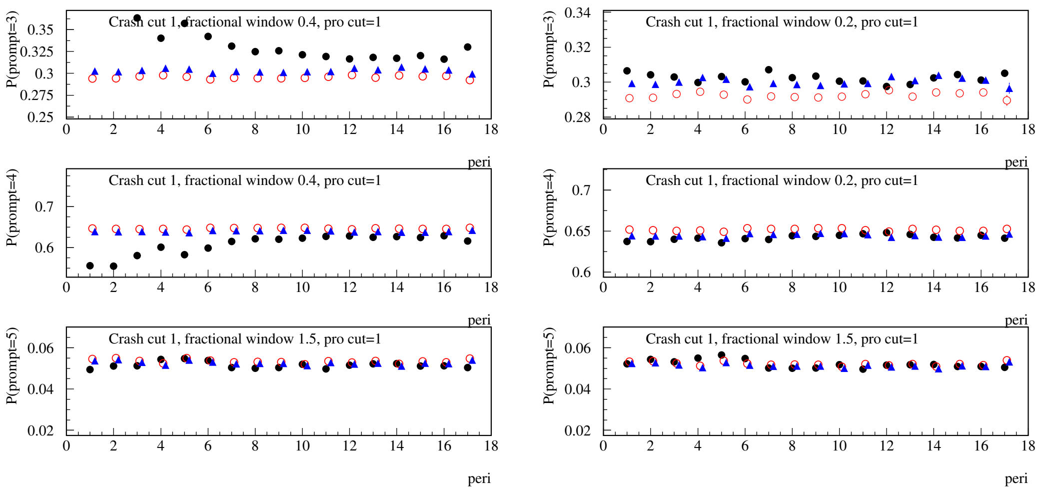

Figure 32: $N_3/N_{\geq 3}$, $N_4/N_{\geq 3}$, $N_5/N_{\geq 3}$ before (left panel) and after (right panel) the splash rejection cut; black = data, open red = MC, blue = MC after cluster efficiency correction.

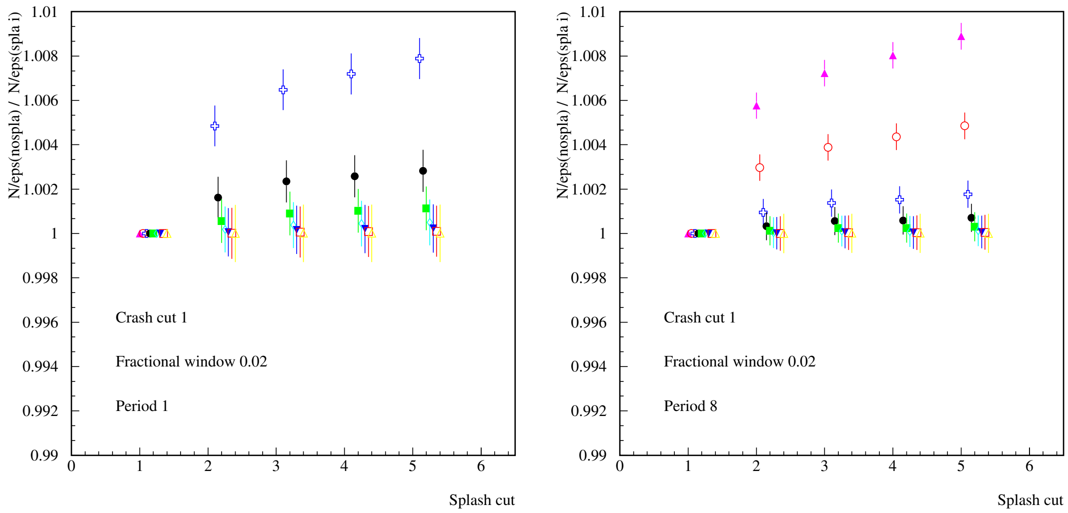

Figure 33: Behaviour of Q for a period of 2001 (left panel) and 2002 (right panel) data taking. Black dots correspond to $\mathrm{E}_\gamma > 20\,\mathrm{MeV}$.

The values of the correction to the measurement, $1/(1 - B_4/S)$, are shown as a function of the data taking period in Fig. 34. The systematic error from splash background subtraction is given by the difference between results obtained with and without applying this correction, and it is 0.07×10^{-3} for $E_{\rm cr} = 300\,\mathrm{MeV}$.

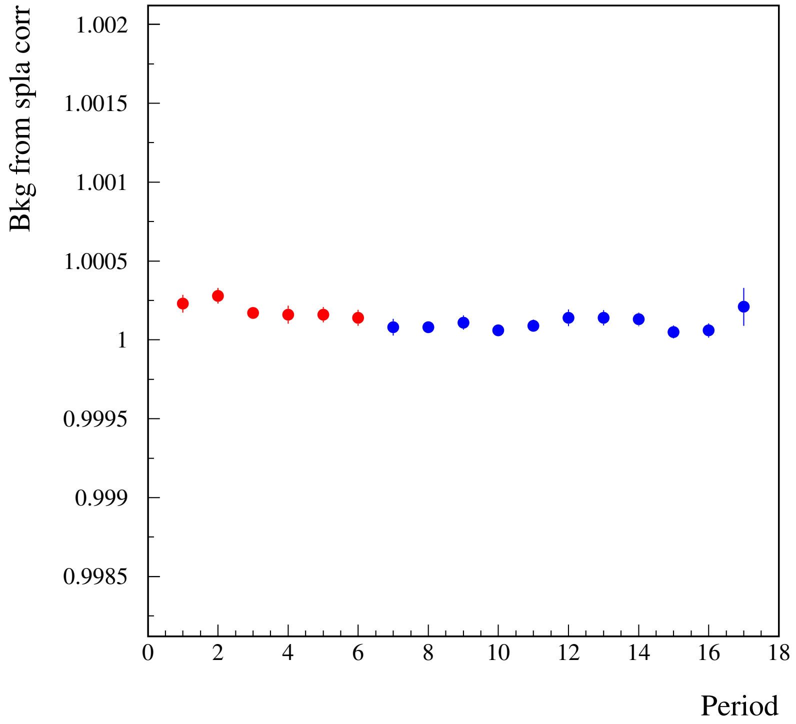

Figure 34: Correction to the result due to residual splash event contamination, as a function of the data taking period.

4.6 $\pi^0\pi^0$selection efficiency

In Fig. 35 we finally present the $\pi^0\pi^0$ acceptance as a function of data taking period. During 2001 (red points) the acceptance suffered because of a higher level of background with more unstable machine conditions. This produced a lower average efficiency with variations of order 1%. In Tab. 5 the values of the $\pi^0\pi^0$ acceptance are reported for the

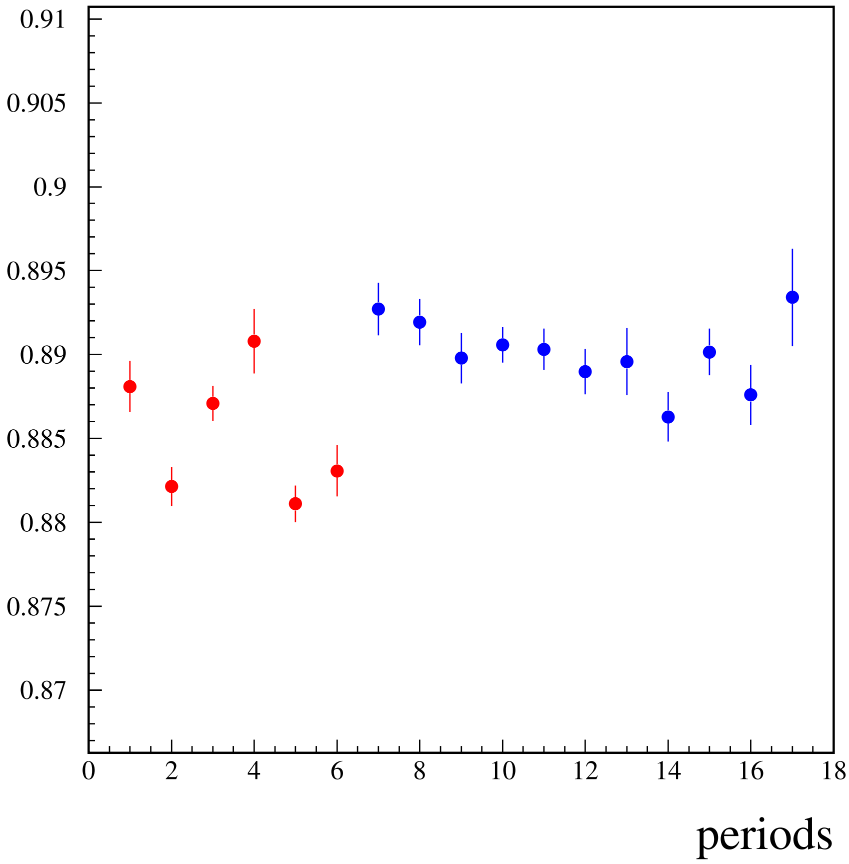

Figure 35: $\pi^0\pi^0$ acceptance as a function of data taking period; red = 2001, blue = 2002.

reference period # 10, for $K_{\rm cr}$-events (a_{cr}) and non-$K_{\rm cr}^{\rm true}$ events ($a_{\overline{cr}}$) separately. Acceptance dependence on $K_{\rm cr}$ energy cut is less than one per-mil.

In Tab. 10 of Sec. 10 we report all of the contributions to the systematic error on the

	a_{cr}	$a_{\overline{cr}}$
$E_{\rm cr} > 125\,{\rm MeV}$	0.8903(7)	0.8807(7)
$E_{\rm cr} > 200\,{\rm MeV}$	0.8910(8)	0.8816(7)
$E_{\rm cr} > 300\,{\rm MeV}$	0.8909(9)	0.8828(7)

Table 5: $\pi^0\pi^0$ acceptance on period # 10.

$\pi^0\pi^0$ acceptance which have been discussed in the previous sections, for the three values of $E_{\rm cr}$ separately.

5 $K_S \to \pi^+\pi^-(\gamma)$: signal selection and acceptance evaluation

In this section we review the selection criteria to isolate the $\pi^+\pi^-$ signal and the method we used to evaluate the acceptance. The present description will on the new features of the analysis. For further details refer to [4], [7], [10] and [2].

Starting from the sample of K_{cr} events, $K_S \to \pi^+\pi^-(\gamma)$ decays are selected by identifying two charged pions from the interaction region (IP). A set of cuts define a pion track from IP:

- Require $\rho_{\text{first}} < 41\,\text{cm}$, $|\text{z}_{\text{PCA}}| < 10\,\text{cm}$, $\rho_{\text{PCA}} < 4\,\text{cm}$, where ρ_{first} is the transverse position of the first hit of the track, and z_{PCA} and ρ_{PCA} are the longitudinal and transverse position of its point of closest approach to the origin.
- Require extrapolation of the track tree to the calorimeter surface with impact point transverse position $\rho_{\text{ext}} > 60\,\text{cm}$; this is the same request for the event T_0 determination.
- Reject kinks with long secondary tracks (> 15 hits) which are not compatible with $\pi \to \mu\nu$ decay kinematics and are not recognized as fake vertices (*i.e.* the missing momentum at the vertex is above 10 MeV).
- Require $\cos\theta < 0.866$ and $120\,\text{MeV}/c < \text{p} < 300\,\text{MeV}/c$.

Events are selected with exactly two oppositely charged tracks from the IP. As a further request, at least one of them must have an associated cluster which is able to provide the event T_0 ($\rho_{\text{CL}} > 60\,\text{cm}$, $E_{\text{CL}} > 50\,\text{MeV}$).

The selection efficiency is evaluated from MC, which includes the effect of photon radiation in the final state [1]. The generator does not apply any cut on the photon energy in the kaon center of mass system. The simulation thus provides a fully inclusive selection efficiency without the need of any *ad hoc* correction; on the contrary, we applied a correction of $\sim 0.3\%$ in the published analysis, [7].

To avoid systematic errors due to possible difference of detector efficiencies between data and MC, the pure MC calculation is corrected by weighting the contribution of each single pion with the ratio of data and MC tracking efficiencies, ${\epsilon_{\rm trk}}^{\rm data}/\epsilon_{\rm trk}^{\rm MC}$. The single-track efficiency $\epsilon_{\rm trk}$ for data and MC are evaluated in bins of trasverse and longitudinal track momenta, $\rm p_T$ and $\rm p_z$, on control samples (see Sec. 5.1). The ratio $\epsilon_{\rm trk}$(data)/$\epsilon_{\rm trk}$(MC) is then folded in the calculation according to the simulated kinematics.

The efficiency $\epsilon_{\rm T0}$ for a single pion with impact on the calorimeter to provide a T_0-cluster is evaluated on various data control sample, it is parametrized in terms of the track momentum and the angle of impact on the EmC, distinguishing π^+ and π^- tracks (or μ^+ and μ^-, in case of pion in flight decays), and treating separately tracks with impact on the barrel or endcap regions. The $\epsilon_{\rm T0}$ efficiency is inserted to correct the MC calculation, as well. The acceptance a_{cr} ($a_{\overline{cr}}$) of the selection efficiency given (vetoed) a $K_{\rm cr}^{\rm true}$ tag is then computed as follows:

$$a_{cr(\overline{cr})} = \frac{1}{N_{cr(\overline{cr})}} \times \sum_{\{i\}} \frac{\epsilon_{\rm trk}^{\rm data}}{\epsilon_{\rm trk}^{\rm MC}} \left(p_{T,1}, p_{z,1}\right) \frac{\epsilon_{\rm trk}^{\rm data}}{\epsilon_{\rm trk}^{\rm MC}} \left(p_{T,2}, p_{z,2}\right) \left[\epsilon_{\rm T0}^{\rm data}\left(p_1, \theta_1\right) \oplus \epsilon_{\rm T0}^{\rm data}\left(p_2, \theta_2\right)\right], \tag{3}$$

where $N_{cr(\overline{cr})}$ is the total number of events having (not having) a $K_{\rm cr}^{\rm true}$ tag (see Sec. 2), $\{i\}$ represents the subsample of those with two tracks selected, and the last term between parentheses represents the OR of the $\epsilon_{\rm T0}$'s for the two tracks ($a \oplus b = a + b - ab$).

5.1 Tracking efficiency

The tracking efficiency $\epsilon_{\rm trk}$ is evaluated from control samples of $K_{\rm cr}$ events. The knowledge of K_S momentum from the tag ($\rm p_S = p_\phi - p_L$) allows us to select a *tagging* track from $K_S \to \pi^+\pi^-$ decay by cutting on the pion momentum in the kaon rest frame: we require $201 < \rm p^* < 209\,MeV$. This selection reduces the background to a negligible level; for each event, a good estimator for the momentum of the other pion is obtained by kinematic closure (refer to [7] for further details).

The single track efficiency is then obtained by counting the fraction of times in which a second track is found, having opposite sign and satisfying the quality cuts listed in the previous section. The efficiency is obtained in bins of transverse and longitudinal estimated momentum, p_T and p_z, and distinguishing for the particle sign.

To the purpose of minimizing the disturbance from tracks belonging to K_L late decays ("track interference effect", see Sec. 1.5) the control sample is selected by requiring $E_{\rm cr} = 300\,\mathrm{MeV}$. This rejects almost all of the late K_L decays, while retaining K_L truly interacting in the calorimeter. The same method has been applied to both data and MC events, in order to evaluate the ratio $\epsilon_{\rm trk}^{\rm data}/\epsilon_{\rm trk}^{\rm MC}$ of Eq. 3. This is shown in Fig. 36 as a function of $\rho_{\rm first}$ (left panel) and of $\rm p_T$ (right panel), for positive and negative pion tracks separately.

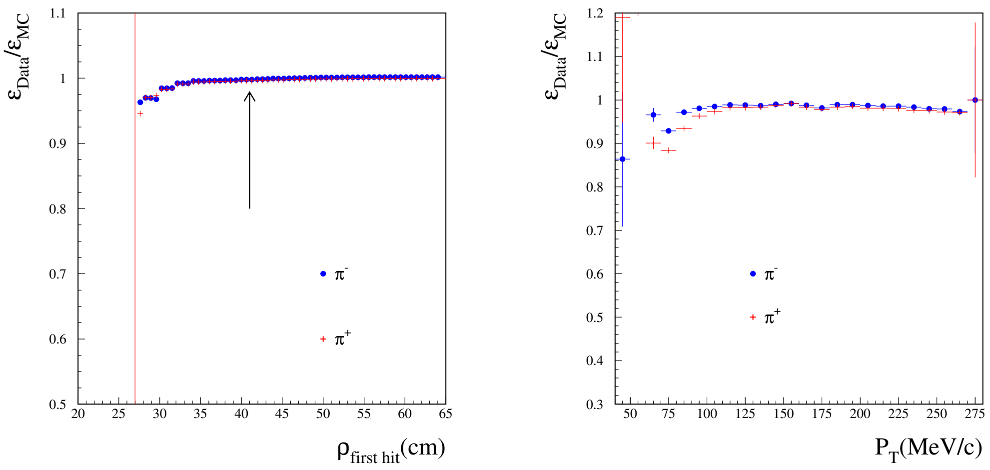

Figure 36: Ratio of tracking efficiencies $\epsilon_{\rm trk}^{\rm data}/\epsilon_{\rm trk}^{\rm MC}$ as a function of $\rho_{\rm first}$ (left panel) and $\rm p_T$ (right panel) for positive (red) and negative (blue) pion tracks.

The new features of the simulation, such as the addition of accidental background hits to the event and the insertion of the measured hardware efficiency to sample the MC hit generation, improved the agreement between data and MC respect to previous versions of the MC code. As a result, $\epsilon_{\rm trk}^{data}/\epsilon_{\rm trk}^{MC}$ reaches a plateau value close to 0.98. Most importantly, the ratio has a flat behavior in the region where the cut on $\rho_{\rm first}$ is applied.

5.2 $\pi^+\pi^-$ selection efficiency

In Fig. 37 (left panel), we present the $\pi^+\pi^-$ acceptance a_{cr} as a function of the data taking period. During 2001 (red points) the variations on a_{cr} are due to high and unstable level of background (compare with the accidental probability, lower panel of Fig. 25). This produced fluctuations of the order of 1%. The relative correction to the MC acceptance induced by the insertion of data-MC track efficiency ratio and T_0 efficiencies from data is shown in the right panel of Fig. 37. In Tab. 6, values of the $\pi^+\pi^-$ acceptance are reported

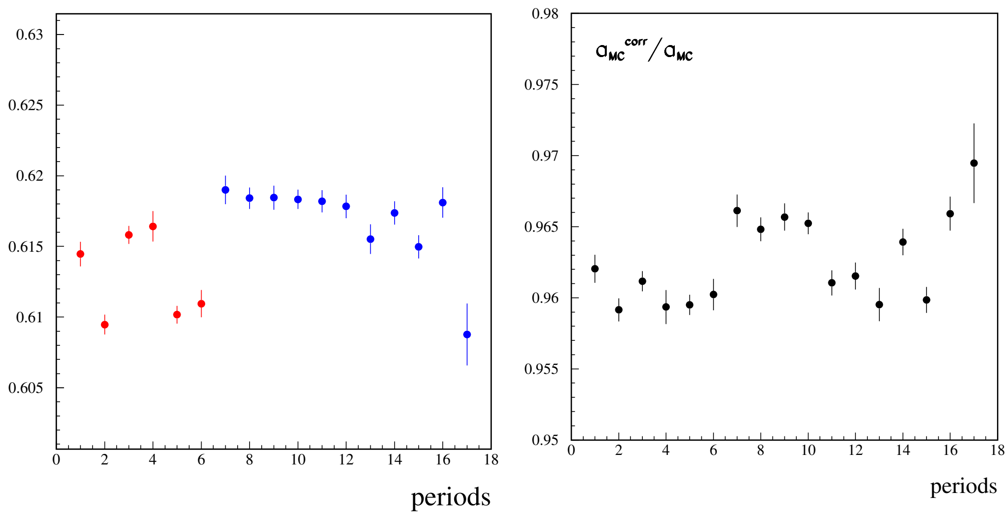

Figure 37: Left panel: $\pi^+\pi^-$ acceptance as a function of data taking period; right panel: ratio between corrected acceptance and pure MC result.

for the reference period # 10, separately for $K_{\rm cr}^{\rm true}$ events (a_{cr}) and non-$K_{\rm cr}^{\rm true}$ events ($a_{\overline{cr}}$). The quoted error refers to the statistics of the MC sample and of the control samples (data and MC) for the efficiency determination. The systematic error will be addressed in the following discussion.

The interference effect, *i.e.* the disturbance between tracks from K_S and K_L late decays, is taken into account in the simulation used to compute the selection efficiency. Indeed, the single-track efficiency corrections are free from interference effect, while the events used to compute the selection efficiency are K_L-crash tagged as in data, thus in-

	a_{cr}	$a_{\overline{cr}}$
$E_{\rm cr} > 125\,{\rm MeV}$	0.6187(5)	0.5968(5)
$E_{\rm cr} > 200\,{\rm MeV}$	0.6192(6)	0.5991(5)
$E_{\rm cr} > 300\,{\rm MeV}$	0.6195(8)	0.6016(5)

Table 6: $\pi^+\pi^-$ acceptance on period # 10.

cluding the correct fraction of K_L late decays.

This is more correct with respect to what we made in the published analysis. In that case, we computed $\epsilon_{\rm trk}^{\rm data}$ cutting on $E_{\rm cr}$ above 100 MeV, thus including some interference in the data single-track efficiency. On the contrary, the single-track MC efficiency $\epsilon_{\rm trk}^{\rm MC}$ and the selection efficiency have been obtained from sample of events with K_L vertex in the calorimeter, thus not allowing for any K_L-K_S interference.

The average difference between the selection efficiency obtained for $E_{\rm cr} = 125\ {\rm MeV}$ and $E_{\rm cr} = 300\ {\rm MeV}$ is 0.8×10^{-3} and it is conservatively assumed as a systematic error on the simulation of K_L-K_S track interference effect.

In order to check the reliability of the T_0 efficiency correction $\epsilon_{\rm T0}$, we applied the same method of Eq. 3, using MC events in place of the data control samples. This is equivalent to evaluate the following average:

$$a_{cr} = \frac{1}{N_{cr}} \times \sum_{\{i\}} \left[\epsilon_{\rm T0}^{\rm MC}\left(p_1, \theta_1\right) \oplus \epsilon_{\rm T0}^{\rm MC}\left(p_2, \theta_2\right)\right], \qquad (4)$$

The result is then compared with the true value of the acceptance, as shown in Fig. 38. The difference is 1.4×10^{-3} for $E_{\rm cr} = 300\,{\rm MeV}$ and it is used to correct the estimate of Eq. 3. The entire correction is taken as systematic error on the selection efficiency.

5.3 Effect of accidental clusters on $\pi^+\pi^-$ selection efficiency

As in the case of the evaluation of the selection efficiency for $\pi^0\pi^0$ decays, the presence of accidental clusters from the machine has to be considered as a possible source of systematic error on the result. Since the value of $T_0^{\rm ev}$ is used in the calculation of DC drift

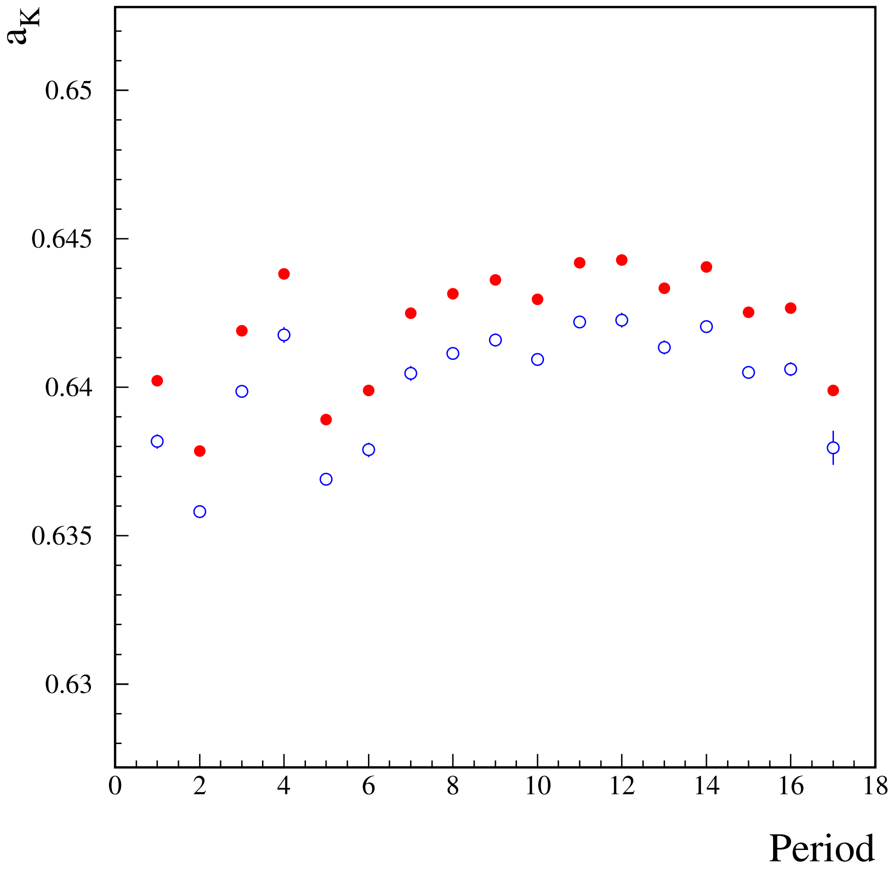

Figure 38: Values of the $\pi^+\pi^-$ acceptance a_{cr} evaluated using the calculation of Eq. 4 (filled dots) are compared with the true-MC values (open dots) as a function of the data taking period.

times, a background cluster "stealing" the T_0^{ev} to the clusters from the event can affect the efficiency and the quality of the reconstructed pion tracks. While in the case of $\pi^0\pi^0$ events a wrong T_0^{ev} causes the direct loss of the event, the $\pi^+\pi^-$ acceptance decreases almost linearly as the time of the accidental T_0-cluster becomes smaller (Fig. 39).

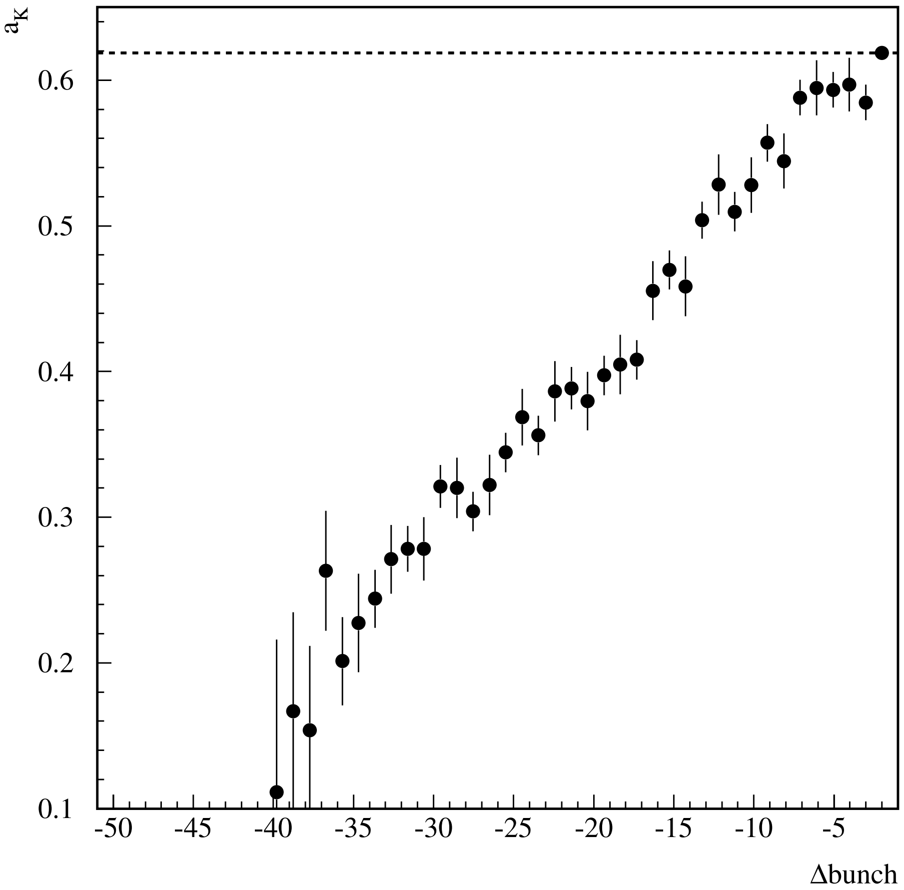

Figure 39: Selection efficiency for $\pi^+\pi^-$ events (Eq. 3) as a function of $\Delta_{\text{bunch}} = (T_0^{\text{ev}} - T_0^{\text{true}})/T_{\text{RF}}$. The last point on the right refers to the average efficiency for $\Delta_{\text{bunch}} > -3$.

Since the rate of accidental clusters extracted from data and inserted into the MC simulation was overestimated due to a bug, we have to correct the $\pi^+\pi^-$ acceptance accordingly. As stated in Sec. 4.2, for the evaluation of $\pi^0\pi^0$ acceptance, we used a set of correction factors F to downscale the rate of accidental clusters with $\Delta_{\text{bunch}} < -2$ ("tail" region, in the following), in order to match that observed in data for $\pi^0\pi^0$ events. We computed the acceptance for $\pi^0\pi^0$ using the corrected T_0 spectrum. For technical reasons, we couldn't repeat the tracking reconstruction with the corrected T_0 spectrum. Therefore, the correction on the $\pi^+\pi^-$ selection efficiency is computed offline, by using the observed behavior of fig. 39, the probability P_{tail} to lie in the tail, and the set of correction factors F:

$$\frac{a_{\text{MC}}^{\text{corr}}}{a_{\text{MC}}}(F) = \frac{\epsilon_{\text{tail}} P_{\text{tail}}/F + \epsilon_{\text{peak}}(1 - P_{\text{tail}}/F)}{\epsilon_{\text{tail}} P_{\text{tail}} + \epsilon_{\text{peak}}(1 - P_{\text{tail}})}, \tag{5}$$

where ϵ_{tail} (ϵ_{peak}) is the average efficiency in the region $\Delta_{\text{bunch}} < -2 (\geq -2)$. To give an order of magnitude of the expected correction, we report the numbers relative to period #10: P_{tail} was $\sim 1.5\%$ in the original MC, and it was overestimated by a factor of $F \sim 2$; the average efficiency is $\epsilon_{\text{tail}} \sim 44\%$ in the tail region, as opposed to $\epsilon_{\text{peak}} \sim 60\%$ in the peak region. Therefore, we should correct the MC selection efficiency by ~ 1.002.

The F factors and the P_{tail} probabilities before and after the correction are shown as a function of the data taking period in left and right panels of Fig. 40, respectively.

The amount of the effect obviously depends on the behavior of the efficiency as a function of the actual value of T_0^{ev}. Since this behavior in turns is related to the tracking response, we can expect to have a different effect for data than for MC. This is checked by selecting a subsample of events with a K_{cr} tag and the $\pi^+\pi^-$ selection, requiring in addition to have a T_0 cluster connected to one of the pion tracks. This cluster gives the true value of the T_0 for both data and MC, ${T_0}^{\text{true}}$. We define $\Delta_{\text{bunch}} = (T_0^{\text{ev}} - T_0^{\text{true}})/T_{\text{RF}}$. The fraction of events $Q^{\text{data(MC)}}$ with $\Delta_{\text{bunch}} < -2$ is shown in Fig. 41, as a function the data taking period, for data and MC. The Q fractions can be expressed as $P_{\text{tail}}\epsilon_{\text{tail}}/\langle\epsilon\rangle$. The large fractional difference between Q^{data} and Q^{MC} observed for 2001 is interpreted as a difference in ϵ^{tail} and it is added to the formulation of Eq. 5 in the evaluation of the correction:

$$\frac{a_{\text{MC}}^{\text{corr}}}{a_{\text{MC}}}(F) = \frac{\epsilon_{\text{tail}} P_{\text{tail}}/F + \epsilon_{\text{peak}}(1 - P_{\text{tail}}/F)}{\epsilon_{\text{tail}} P_{\text{tail}} + \epsilon_{\text{peak}}(1 - P_{\text{tail}})} + Q^{\text{data}} - Q^{\text{MC}}. \tag{6}$$

The final correction (Eq. 6) is shown in Fig. 42 as a function of the data taking period. As expected, this correction is higher in the case of 2001 data.

We now turn to the problem of assigning a systematic error to the correction discussed

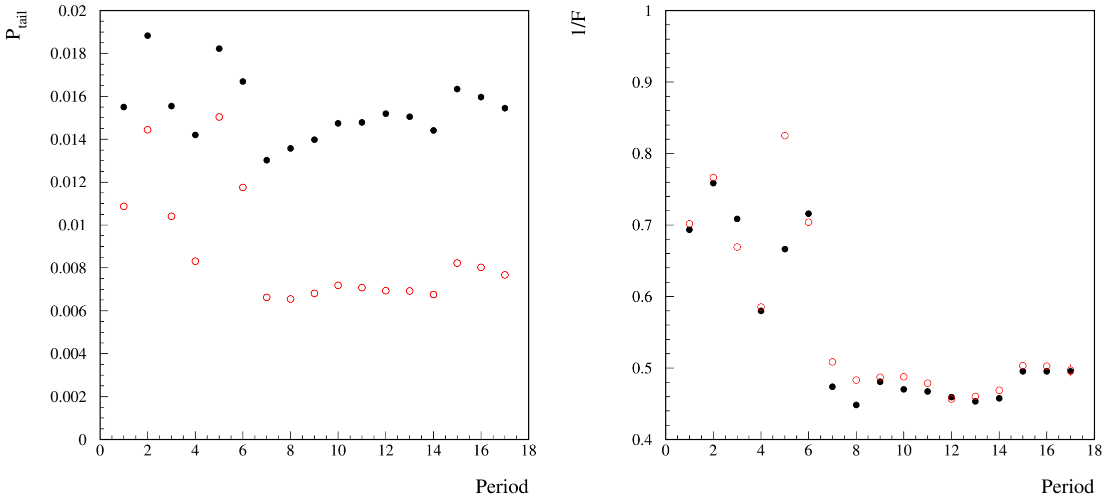

Figure 40: Left panel: probability for a $\pi^+\pi^-$ event to have T_0 in the tail region, before (filled dots) and after (open dots) the downscaling of accidental clusters ($\times 1/F$) is applied. Right panel: the correction factors $1/F$ (solid black dots) and the ratio of the $P_{\rm tail}$ probabilities before and after the correction.

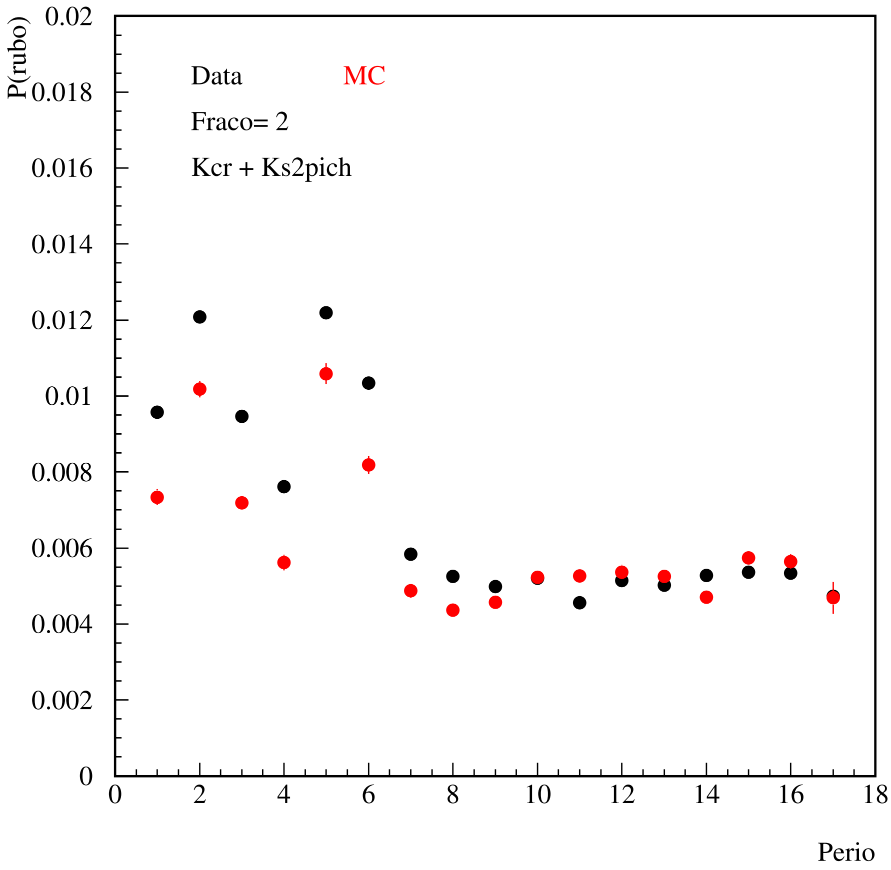

Figure 41: $Q^{\rm data}$ (black dots) and $Q^{\rm MC}$ as a function of the data taking period.

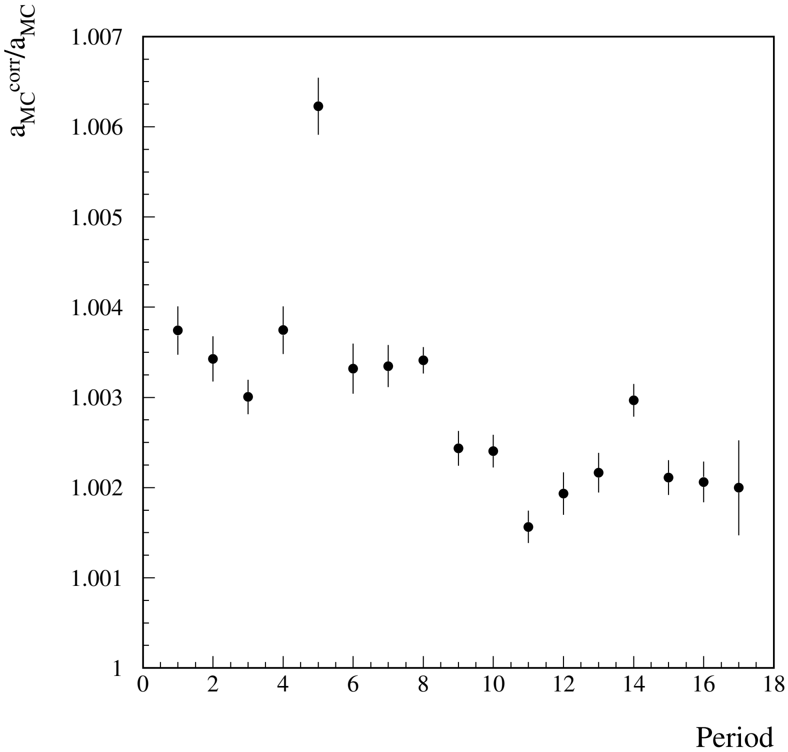

Figure 42: Final correction to the $\pi^+\pi^-$ selection efficiency, Eq. 6, as a function of the data taking period.

above. First of all the correction itself is obtained under the assumption that switching off an accidental cluster in the tail will shift the event to the peak region. This is not true if the accidental cluster is the only T_0-cluster in the event: the rest of the event has not a T_0^{ev} determination and therefore cannot be selected at all. This effect is measured to be smaller than 10^{-4}.

A further effect arises if a second accidental T_0-cluster lying in the tail region survives the downscaling. In this case, the event will remain in the tail region after the correction. This can be taken into account if in place of the F-factors in Eq. 6 we use the ratio of tail probabilities before and after the downscaling on accidentals is applied (shown in left panel of Fig. 40). The average difference between the two evaluations of the correction is $\sim 3 \times 10^{-4}$ and it is taken as a systematic error (almost flat with respect to E_{cr}).

Finally, the reliability of the F-factors used to correct the MC has been checked using the 5-prompt sample of selected $\pi^0\pi^0$ events. As explained in Sec. 4.2, the difference between data and MC probabilities for single accidental clusters to became prompt photons, P_{acci} (right panel of Fig. 25) can be used to evaluate a correction to the acceptance (right panel of Fig. 26). Similarly, we evaluate the correction to Eq. 6 by using $F^* = F \times P_{\mathrm{acci}}^{\mathrm{data}} / P_{\mathrm{acci}}^{\mathrm{MC}}$ in place of F. The fractional variation is shown in left panel of Fig. 43. Since this correction is correlated with that evaluated for the $\pi^0\pi^0$ acceptance, we show the ratio R_{acci} of the two corrections in the right panel of Fig. 43. The difference between the final results obtained correcting for R_{acci} or not is $\sim 4 \times 10^{-4}$ (almost flat with respect to E_{cr}).

The systematic error on the measurement due to the accidental rate is obtained by summing in quadrature the above mentioned errors, and is $\sim 0.5 \times 10^{-3}$.

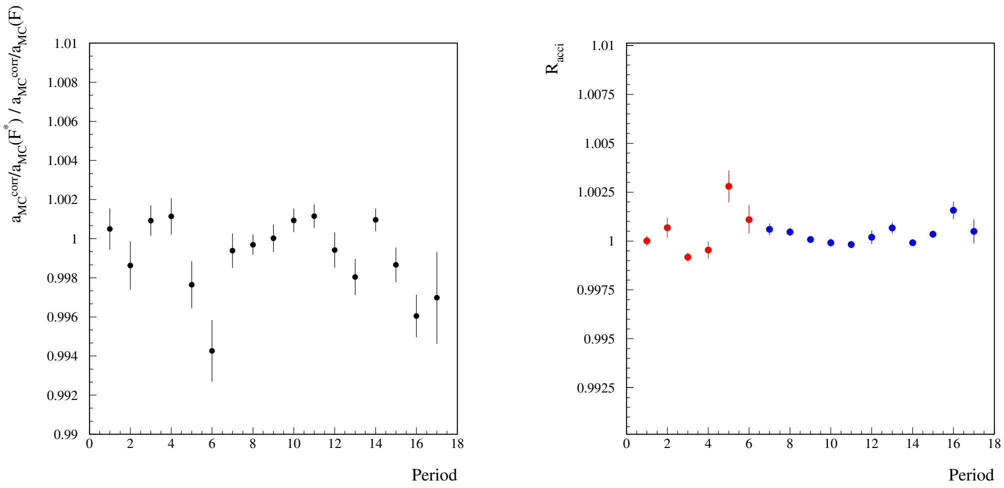

Figure 43: Left panel: $\frac{a_{\rm MC}^{\rm corr}}{a_{\rm MC}}\left(F^{*}\right) / \frac{a_{\rm MC}^{\rm corr}}{a_{\rm MC}}\left(F\right)$ as a function of the data taking period; right panel: $R_{\rm acci}$ as a function of the data taking period.

6 Trigger efficiency

The methods used for the estimate of the trigger efficiency corrections are here briefly described. For a more detailed description, see [7].

The main method for the trigger efficiency evaluation ("hemisphere" method in the following) uses data samples of the selected events, *i.e.* events with a $K_{\rm cr}$ tag and satisfying the $\pi^0\pi^0$ or the $\pi^+\pi^-$ selection. Each cluster in the event is assigned to K_S or K_L "hemisphere" according to the difference δ_t of the cluster time with respect to the $K_{\rm cr}$ cluster: for $\pi^0\pi^0(\pi^+\pi^-)$ decays, if $\delta_t < -15(-2)$ ns, the cluster is assigned to K_S, otherwise to K_L.

The idea is then to extract the probability $P^{(i)}_{L(S)}$ for the $K_L(K_S)$ to fire i trigger sectors by requiring that the trigger condition be satisfied by the set of $K_S(K_L)$ clusters. The event trigger efficiency is then calculated combining K_S and K_L trigger sector probabilities. Since K_L practically always fires at least one trigger sector, we have:

$$\epsilon^{\rm hem}_{\rm trg} \sim 1 - P^{(0)}_S P^{(1)}_L \tag{7}$$

Results from this method are shown in Fig. 44 for $\pi^0\pi^0$ (left panel) and $\pi^+\pi^-$ (right panel), as a function of the data taking period. The variations observed are due to actual variations in the effective energy threshold of the calorimeter sectors.

In order to check the reliability of the hemisphere method, we applied it to a sample of MC events and we compared the result with the trigger efficiency from MC truth, $\epsilon^{\rm true}_{\rm trg}$. The ratio of the two quantities is shown in left panel of Fig. 45 for $\pi^0\pi^0$ and $\pi^+\pi^-$ events. This ratio is used to correct the $\pi^+\pi^-$ efficiency, the only showing a small bias ($< 10^{-3}$). The corresponding variation of the result is taken as systematic error and it is $\sim 0.4\times10^{-3}$ for $E_{\rm cr} = 300\,{\rm MeV}$.

A different method ("single particle" in the following) is also applied for $\pi^+\pi^-$ events, using MC events weighted with single-particle trigger sector efficiencies $\varepsilon_{\rm sec}$ taken from various data control samples. These are parametrized in terms of kinematic quantities, also distinguishing for the particle type and the detector hit. The probability $P^{(0)}_S$ is then calculated and combined with $P^{(1)}_L$ taken from data. This method does not include the effect on the trigger of accidental clusters. Moreover, the effect of two K_S pions con-

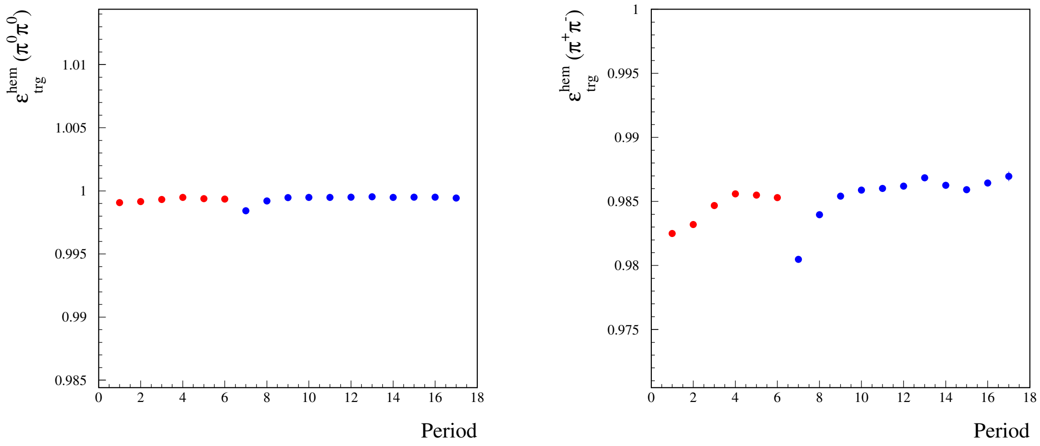

Figure 44: Trigger efficiency for $\pi^0\pi^0$ (left) and $\pi^+\pi^-$ events (right) as a function of the data taking period.

tributing with their energies to the same trigger sector is not present as well. In these events each of the two pion energy can be below the threshold, but the combined sum of the energies is able to fire the trigger sector. Both effects lead to an underestimated value for the efficiency. The ratio of efficiencies obtained with the hemisphere and the single-particle methods is shown for data and MC in the right panel of Fig. 45. The MC reproduces these effects, but with a $< 0.2\%$ difference for the 2002 data sample. We don't apply any correction for this. We use instead this data-MC difference as a systematic error on the trigger efficiency. The average value of this error on the whole data set is 0.62×10^{-3} for $E_{\rm cr} = 300\,\mathrm{MeV}$.

The total systematic error on the trigger efficiency evaluation is obtained by summing in quadrature the above mentioned errors, and is 0.67×10^{-3} for $E_{\rm cr} = 300\,\mathrm{MeV}$.

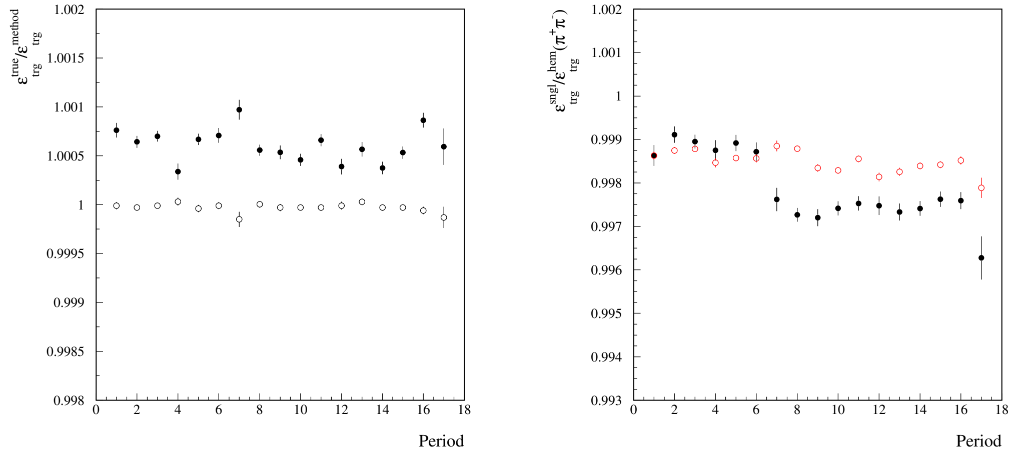

Figure 45: Left panel: $\epsilon^{\rm true}/\epsilon^{\rm hem}$ on MC events, for $\pi^+\pi^-$ (filled dots) and $\pi^0\pi^0$ (open dots) decays, as a function of the data taking period; right panel: $\epsilon^{\rm sngl}/\epsilon^{\rm hem}$ for $\pi^+\pi^-$ events, for data (filled dots) and MC (open dots).

7 Cosmic veto correction

The cosmic veto [12] is responsible for a $\sim 4\%$ loss of the events selected with a $K_{\rm cr}$ tag. To identify a cosmic ray the veto makes a hardware sum of the energy released in the outermost layer of the calorimeter, and requires two sectors fired with energy deposition above 30 MeV. The $K_{\rm cr}$ cluster is able to trigger a single cosmic sector in $\sim 30\%$ of the times. Moreover, in $\sim 2\%$ of the cases the cluster spreads over two contiguous sectors satisfying the veto condition by itself.

During the main part of 2001 data taking, a downscaled fraction $1/(DW_{CR}+1)$ of the vetoed events has been acquired in order to estimate the veto efficiency for every sample of selected events. Starting from the end of 2001, this hardware veto has been disabled ($DW_{CR}=0$), while the events flagged as cosmic rays were sent to a software filter ("T3" filter). The T3 aims at recovering particular categories of physics events, such as $e^+e^- \to \pi^+\pi^-\gamma, \mu^+\mu^-\gamma$, which are frequently mistagged as cosmic rays, by looking for the presence of tracks coming from the IP. The efficiency for this selection is evaluated again by downscaling software a fraction $1/DW_{T3}$ of the events which are still flagged as cosmic rays after T3.

The downscaling factors DW_{CR} and DW_{T3} applied in the various periods of the data taking are listed in Tab. 7, with detail on both the run number intervals and the data taking period defined in our analysis.

Run interval	Run period	DW_{CR}	DW_{T3}
17845-22301	1-4 + 5a	4	1
22302-22827	5b	4	4
22828-23027	6a	4	64
23028-27137	6b + 7-17	0	64

Table 7: Hardware and software downscaling factors for cosmic veto efficiency evaluation.

To evaluate the cosmic veto efficiency we divide the selected events into three categories:

- Events without a hardware cosmic-ray tag (N_0);
- Events flagged as cosmic-rays by hardware, but recovered by T3 (N_1);
- Events flagged as cosmic-rays by hardware and rejected by T3 (N_2).

In our analysis scheme only events without a hardware cosmic-ray flag are retained. The efficiency of this requirement is then evaluated as follows:

$$\epsilon_{\rm CV} = \frac{N_0}{N_0 + (DW_{CR} + 1)(N_1 + N_2 \cdot DW_{T3})} \tag{8}$$

In Fig. 46, we show the values of $\epsilon_{\rm CV}$ for $\pi^0\pi^0$ and $\pi^+\pi^-$ final states. The small variations observed are a consequence of the variations of the hardware trigger sector thresholds (compare with Fig.44). The statistical error on $\epsilon_{\rm CV}$ is $\sim 0.3 \times 10^{-3}$ for a standard period of 2001. During 2002, a difference arises between the two channels. $\pi^+\pi^-$ events are efficiently recovered by T3, while almost all of the $\pi^0\pi^0$ events are rejected. Since DW_{T3} in 2002 is larger than DW_{CR} in 2001, the statistical uncertainty for $\pi^0\pi^0$ events grows up to $\sim 10^{-3}$ for a standard period of 2002, while remaining the same for $\pi^+\pi^-$ events.

The fractional statistical uncertainty due to the cosmic veto correction on the final result is 0.14×10^{-3}, 0.18×10^{-3}, and 0.26×10^{-3} for $K_{\rm cr}$ minimum energies of 125, 200, and 300 MeV, respectively.

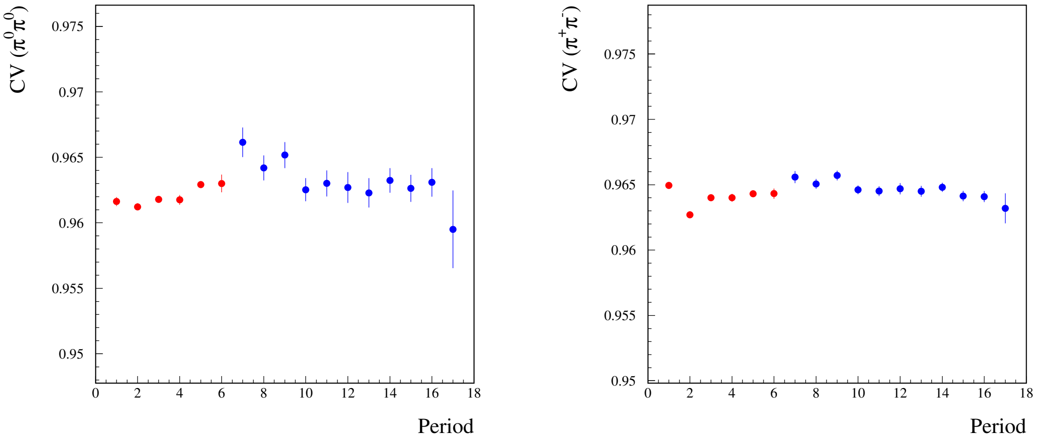

Figure 46: Cosmic veto correction for $\pi^0\pi^0$ events (left panel) and for $\pi^+\pi^-$ events (right panel) as a function of the data taking period.

8 Filfo efficiency

The FILFO algorithm is a software filter designed to reject machine background events and residual cosmic-ray events through the analysis of calorimeter information before the tracks are reconstructed. The FILFO inefficiencies $1 - \epsilon_{\rm FILFO}^{\rm MC}$ are predicted by MC to be smaller than 10^{-3} for both $\pi^+\pi^-$ and $\pi^0\pi^0$, throughout the entire data set (open dots in Fig. 47).

In order to check the reliability of this prediction, we used a subsample of 5 periods within 2002 data set, for which the FILFO output is registered but not enforced for a downscaled fraction of the events. The FILFO efficiency $\epsilon_{\rm FILFO}^{\rm DATA}$ for $\pi^+\pi^-$ and $\pi^0\pi^0$ samples obtained for these runs are shown again in Fig. 47 (filled dots). The inefficiencies are again smaller than 10^{-3} for both channels. A small correction on the MC prediction is applied to the final result by calculating the average ratio of $\pi^0\pi^0$ and $\pi^+\pi^-$ efficiencies for data and MC:

$$R_{\rm FILFO} = \frac{\epsilon_{\rm FILFO}^{\rm data}(\pi^0\pi^0)/\epsilon_{\rm FILFO}^{\rm data}(\pi^+\pi^-)}{\epsilon_{\rm FILFO}^{\rm MC}(\pi^0\pi^0)/\epsilon_{\rm FILFO}^{\rm MC}(\pi^+\pi^-)} \tag{9}$$

The values of $R_{\rm FILFO}$ are listed in Tab. 8 as a function of the cut on the $K_{\rm cr}$ energy. We use the entire value of the correction as an estimate of the systematic error.

$K_{\rm cr}$ energy cut (MeV)	$R_{\rm FILFO} - 1$	$\chi^2_{\rm fit}/\#DOF$	$P(\chi^2 > \chi^2_{\rm fit}$
125	$(4.5 \pm 0.3) \times 10^{-4}$	35/39	62%
200	$(4.6 \pm 0.3) \times 10^{-4}$	40/39	37%
300	$(7.4 \pm 0.5) \times 10^{-4}$	38/39	46%

Table 8: Correction $R_{\rm FILFO}$ due to data-MC difference for the FILFO efficiency as a function of the $K_{\rm cr}$ minimum energy. The χ^2 value of the fit to a constant and the associated probabilities are also shown.

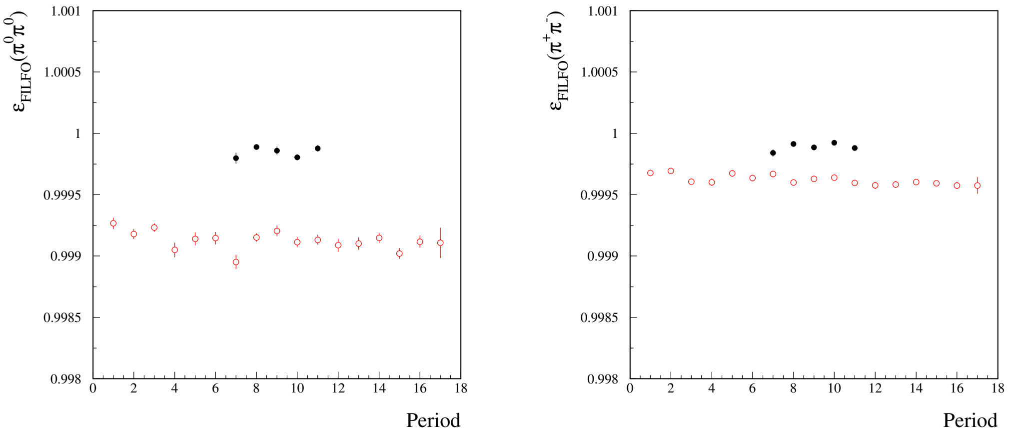

Figure 47: Efficiency of the FILFO algorithm as a function of the data taking period, on $\pi^0\pi^0$ (left panel) and $\pi^+\pi^-$ (right panel) events; the prediction from MC (open dots) is compared with that obtained from data (filled dots) on a subsample taken in year 2002.

9 Background from other ϕ decays

The contamination from other ϕ decays gives a sizeable correction to the final result.

The contamination of the $\pi^+\pi^-$ sample is estimated by MC to be $\sim 1.1 \times 10^{-3}$ (see left panel of Fig.48), flat with respect to the cut on $E_{\rm cr}$. Two sources are contributing: K_S decays to semileptonic final states ($\sim\ 0.7 \times 10^{-3}$) and $\phi \to \pi^+\pi^-\pi^0$ decays ($\sim 0.4 \times 10^{-3}$).

Semileptonic decays are able to satisfy with high efficiency our loose selection criteria. The uncertainty on this background component is 5% from the knowledge of K_S semileptonic branching ratios (uncertainty on $K_{S,\mu 3}$ decay is assumed to be equal to that on $K_{S,e3}$, although it is not measured yet), and 5% from the acceptance evaluation.

Decays $\phi \to \pi^+\pi^-\pi^0$ are selected thanks to an accidental cluster stealing the T_0 and making one of the two high-energy photons from the π^0 to be erroneously selected as $K_{\rm cr}$. For this reason the small variations of the purity as a function of the data taking period follow closely the behaviour of the accidental probability (compare with right panel of Fig. 25). A rough calculation can be performed to compute the systematic uncertainty on this component; the ratio between the number of events selected by this mechanism and the number of signal events is evaluated as follows:

$$\frac{N(\phi \to \pi^+\pi^-\pi^0)}{N(K_S \to \pi^+\pi^-)} = \frac{{\rm BR}(\phi \to \pi^+\pi^-\pi^0)}{{\rm BR}(\phi \to K_S K_L){\rm BR}(K_S \to \pi^+\pi^-)} \times \frac{a(\phi \to \pi^+\pi^-\pi^0)}{a(K_S \to \pi^+\pi^-)} \times P_{\rm steal} \tag{10}$$

where $a(i)$ is the total acceptance for channel i and the probability $P_{\rm steal}$ is the probability for an accidental cluster to shift the T_0 within the window suitable for a prompt photon (time of flight of $\sim\ 6$ ns) to satisfy the $K_{\rm cr}$ selection, *i.e.* $-15 < \Delta_{\rm bunch} < -9$. With the values $a(K_S \to \pi^+\pi^-) = 0.3 \times 0.6$ and $a(\phi \to \pi^+\pi^-\pi^0) = 0.06$ (from MC), and $P_{\rm steal} = 1.5 \times 10^{-3}$, we get a contamination of 0.3×10^{-3}, close to what is obtained from the complete background simulation. A conservative estimate of the systematic uncertainty on this component is 20%, corresponding to the fractional error on $P_{\rm steal}$.

Summing in quadrature the systematic errors of both background components we get a fractional error on the contamination of $\sim 9\%$, from which we evaluate an uncertainty of 0.1×10^{-3} on the final measurement, independent of $E_{\rm cr}$.

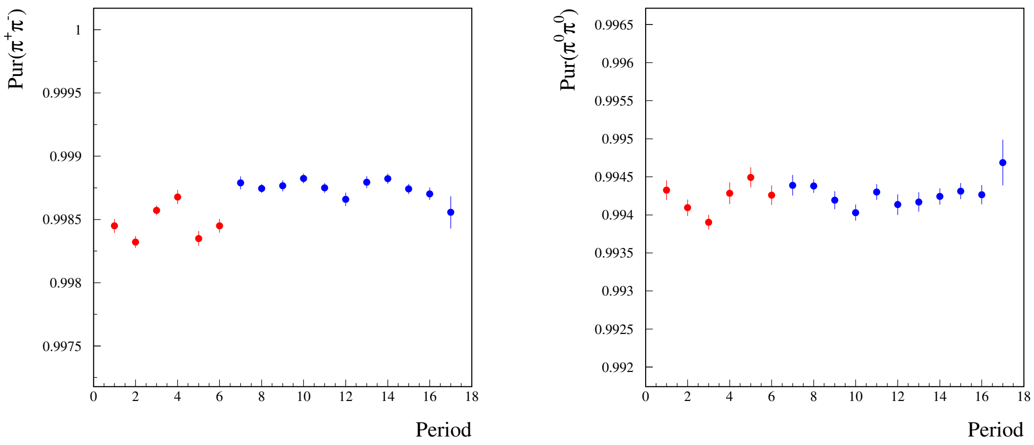

Figure 48: Purity of the $\pi^+\pi^-$ (left) and $\pi^0\pi^0$ (right) samples as a function of the data taking period, for $K_{\rm cr}$ minimum energy of 125 MeV.

The $\pi^0\pi^0$ sample is contaminated mainly by K^+K^- events (we don't apply a track veto in our $\pi^0\pi^0$ selection): one of the two kaons undergoes a prompt τ' decay, while the other decays to π^0's within the drift chamber. If the flight path of this kaon is between roughly 90 and 160 cm, one of the two photons from the π^0 decay can be mistagged as a $K_{\rm cr}$. The ratio between the number of events selected by this mechanism and the number of signal events is evaluated as follows:

$$\frac{N(K^+K^-)}{N(K_S \to \pi^0\pi^0)} = 2 \times \frac{{\rm BR}(\phi \to K^+K^-){\rm BR}(\tau'){\rm BR}(\pi^0)}{{\rm BR}(\phi \to K_SK_L){\rm BR}(\pi^0\pi^0)} \times \frac{P_{\rm early}a(\tau') \times P_{\rm after}a(\pi^0)}{a(K_S \to \pi^0\pi^0)}, \tag{11}$$

where $K^\mp$ undergoes a τ' decay while ${\rm BR}(\pi^0) \sim 30\%$ is the BR for a $K^\pm$ to produce at least one π^0 in the final state; the first decay happens with a flight path shorter than 40 cmwith a probability $P_{\rm early} \sim 40\%$; the acceptance $a(\tau')$ for this decay to produce 3 or more prompt clusters is close to 1. The second decay should happen in the flight path interval $(90, 160)$ cm, so with probability $P_{\rm after} \sim 20\%$. Using an acceptance for having at least one photon on the barrel of $a(\pi^0) = 75\%$ and putting a factor of 2 for the 2-kaon exchange, we get a contamination of $\sim 4 \times 10^{-3}$. This is comparable with the value obtained from a detailed simulation of this background: the contamination is $\sim 6 \times 10^{-3}$ (right panel of Fig. 48), $\sim 2 \times 10^{-3}$, and $< 10^{-3}$ for $K_{\rm cr}$ minimum energies of 125, 200, and 300 MeV, respectively.

Systematic uncertainties in this prediction arise from the error on $\mathrm{BR}(\tau')$, $\sim 3\%$, from $\mathrm{BR}(K^+K^-)$, $\sim 1\%$, and from the uncertainty on the τ' acceptance, which can be estimated of few percent. We conservatively assume a systematic error of 6% on the contamination to $\pi^0\pi^0$ events, which produces an uncertainty on the final measurement of 0.35×10^{-3}, 0.14×10^{-3}, and 0.04×10^{-3} for $K_{\rm cr}$ minimum energies of 125, 200, and 300 MeV, respectively.

10 Results

We report here the formula for the evaluation of the ratio of BR's, discussed in Sec. 2:

$$\frac{\mathrm{BR}(K_S \to \pi^+\pi^-(\gamma))}{\mathrm{BR}(K_S \to \pi^0\pi^0)} = \frac{N(\pi^+\pi^-)}{N(\pi^0\pi^0)} \times \frac{C(\pi^+\pi^-)}{C(\pi^0\pi^0)} \frac{\epsilon_{\mathrm{sel}}(\pi^0\pi^0)}{\epsilon_{\mathrm{sel}}(\pi^+\pi^-)}, \tag{12}$$

where $N(i)$ is the number of selected events for channel i, C is the purity of the selection, and the selection efficiencies ϵ_{sel} for each channel are obtained from the following formula, discussed in Sec. 2:

$$\epsilon_{\mathrm{sel}} = [\, \epsilon_{cr} a_{cr} \sum_n f_n P_n^{in} + (1-\epsilon_{cr}) a_{\overline{cr}} \sum_n f_n P_n^{out} \,] \epsilon_{\mathrm{trg}} \epsilon_{\mathrm{CV}} \epsilon_{\mathrm{FILFO}}. \tag{13}$$

The following quantities in the above formulas are taken from data: the yield ($N(i)$), the ingredients for the evaluation of the K_{cr}-tag efficiency ratio (f_n, P_n^{in}, and P_n^{out}), and the trigger and cosmic-veto efficiencies (ϵ_{trg} and ϵ_{CV}). The following are taken instead from analyses of the MC samples with corrections driven by data: the K_{cr} efficiency given the true T_0 (ϵ_{cr}), the acceptance given or not the K_{cr} tag (a_{cr} and $a_{\overline{cr}}$), and the efficiency of the FILFO filter ($\epsilon_{\mathrm{FILFO}}$). The purity ($C$) is taken from the MC without any correction.

Possible biases in the methods used to extract efficiencies from data are calculated and included as correction by comparing in the MC the method output with the true value. This is done for the trigger and tag-ratio efficiencies. Whenever we extract an efficiency from MC, we take care of including in the calculation possible data-MC discrepancies. This is done for the ratio of K_{cr} efficiencies, the acceptances, and the FILFO efficiency.

In order to avoid statistical correlations between the various quantities taken from data, we split our sample into 3 parts on a random basis (we use the rest of trigger number divided by 3). The first of these is used for event counting, the second for tag-ratio calculation, and the third for the evaluation of the trigger efficiency.

In the case of the corrections taken from MC, we use a sample of ϕ decays equivalent to $0.2 \times 410\ \mathrm{pb}^{-1}$. The statistical correlations between the estimates of ϵ_{cr}, a_{cr}, and $a_{\overline{cr}}$ have been taken into account in the evaluation of the statistical error.

For stability studies the data set is divided into 17 periods and the analysis is performed independently on each of these periods; these are defined (Sec. 1.6) taking into account variations of the data taking conditions: the center of mass energy $\sqrt{s}$ and the rate of accidental clusters from the machine are used for this pourpose; periods are also distinguished if different calibration methods were used and if different trigger conditions were required. The values of all of the quantities appearing in the above formulas are listed in Tab. 9, for period #10 and $K_{\rm cr}$ minimum energies of 125, 200 and 300 MeV.

	$\pi^+\pi^-$			$\pi^0\pi^0$		
$E_{K_{\rm cr}}$ cut	125	200	300	125	200	300
N (10^3)	1 218.00(88)	907.41(74)	490.92(54)	811.79(79)	587.68(66)	312.90(48)
ϵ_{cr}	0.3106(2)	0.2231(2)	0.1082(2)	0.3097(3)	0.2217(3)	0.1067(2)
a_{cr}	0.6187(5)	0.6192(6)	0.6195(8)	0.8905(7)	0.8911(8)	0.8910(9)
$\sum_n f_n P_n^{in}$	0.9634(1)	0.9866(1)	0.9933(1)	1.	1.	1.
$\sum_n f_n P_n^{out}$ (10^{-3})	3.4489(6)	1.6675(1)	0.71563(3)	0.	0.	0.
$\epsilon_{\rm trg}$	0.9863(1)	0.9867(1)	0.9879(2)	0.99948(3)	0.99948(3)	0.99951(4)
$\epsilon_{\rm CV}$	0.9646(3)	0.9626(4)	0.9598(6)	0.9625(9)	0.959(1)	0.954(2)
$\epsilon_{\rm FILFO}$	0.99964(2)	0.99963(3)	0.99944(4)	0.99956(3)	0.99953(3)	0.99937(5)
C	0.99882(4)	0.99891(4)	0.99886(6)	0.9940(1)	0.99761(8)	0.99938(6)

Table 9: Values for the efficiencies quoted in Eq. 13, for period #10 and $K_{\rm cr}$ minimum energies of 125, 200, 300 MeV. Statistical errors are shown in parentheses.

The ratio of the number of selected events for a $K_{\rm cr}$ minimum energy of 300 MeV is shown in left panel of Fig. 49 as a function of these data taking periods; the variations observed are a consequence of the variations in the total efficiencies: the χ^2 of a fit to a constant corresponds to a probability of $\sim 2.4 \times 10^{-7}$. After the corrections of Eq. 12, we obtain the result for the ratio of BR's shown in right panel of Fig. 49. The χ^2 probability of the fit to a constant is very good.

For the calculation of the systematic error, our strategy was twofold. Whenever we apply a correction taken from the analysis of MC (data and MC) samples to an efficiency extracted with some method from data (MC), we vary the amount of the correction by $\pm 100\%$ and we take the corresponding variation in the final result as systematic error. Whenever the data-MC comparison indicates an uncertainty from which is not possible to

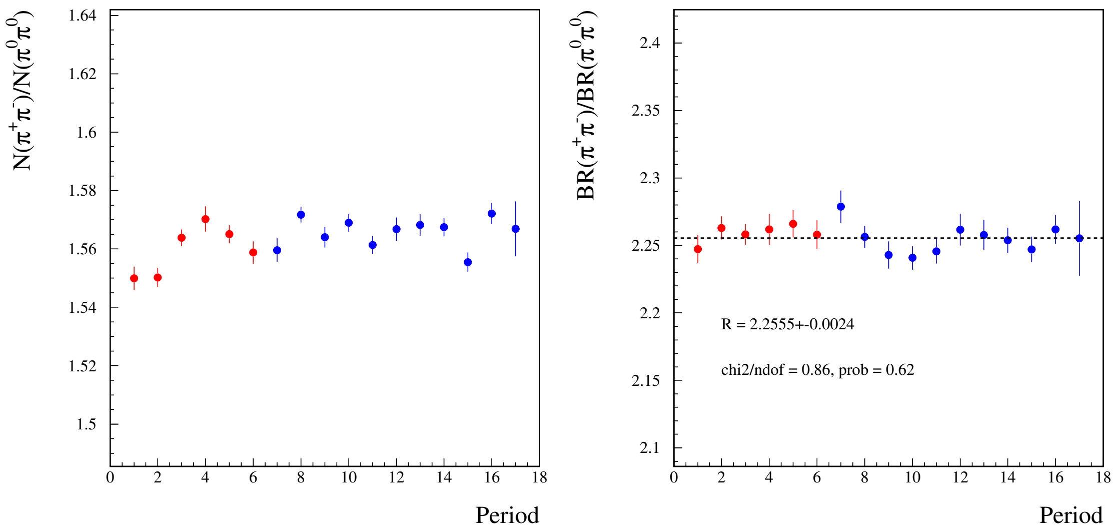

Figure 49: Left panel: ratio of the number of selected $\pi^+\pi^-$ and $\pi^0\pi^0$ events for a minimum $K_{\rm cr}$ energy of 300 MeV, as a function of the data taking period. Right panel: result for $\mathrm{BR}(K_S \to \pi^+\pi^-(\gamma))/\mathrm{BR}(K_S \to \pi^0\pi^0)$ for a minimum $K_{\rm cr}$ energy of 300 MeV, as a function of the data taking period. The error bars represent the statistical error. The result of a fit to a constant and the associated χ^2 are also reported.

derive a correction, we assume as systematic error the uncertainty averaged on the data set. As an example, systematic errors belonging to the last category are the uncertainty in the prompt-cluster counting estimate, the difference between the results from the hemisphere and single-particle methods for the trigger efficiency, the uncertainty in the background contamination from physics events.

The various contributions to the total statistical and systematic errors are disentangled, as shown in Tab. 10 for $E_{\rm cr} = 125, 200$ and $300\ \mathrm{MeV}$.

Some of the efficiencies show variations as a function of the cut on the $K_{\rm cr}$ minimum energy (see Tab. 9): going from $E_{\rm cr} = 125\,\mathrm{MeV}$ to $E_{\rm cr} = 300\,\mathrm{MeV}$ the $K_{\rm cr}$ efficiency ratio, the value of $\sum_n f_n P_n^{in}$ for $\pi^+\pi^-$, and the $\pi^0\pi^0$ contamination grow by $\sim\ 1\%$, $\sim\ 3\%$ and $\sim\ 0.5\%$, respectively. Therefore we check the reliability of these corrections by comparing the results of the analysis for $ecr = 125, 200$ and $300\,\mathrm{MeV}$. Note that the $K_{\rm cr}$ efficiencies drops by a factor 3 in the same interval of $E_{\rm cr}$. The results for $K_{\rm cr}$ energy of 125 and 200 MeV are shown in Fig. 50.

The χ^2 probabilities are good. In order to compare the results for the 3 cuts avoiding correlation effects, we split the data set using a finer granularity, corresponding to 94 micro-periods each of $\sim\ 5\ \mathrm{pb}^{-1}$ of integrated luminosity. The analysis is performed using a different energy cut on each contiguous micro-period. The χ^2 of the 3 values obtained has a marginal probability of 21% (see Tab. 11).

The final result is obtained by minimizing the total error as a function of the $K_{\rm cr}$ energy cut. The best accuracy is for $K_{\rm cr}$ energy cut above 300 MeV, see Tab. 10. The result is:

$$\boxed{\frac{\mathrm{BR}(K_S\to\pi^+\pi^-(\gamma))}{\mathrm{BR}(K_S\to\pi^0\pi^0)} = 2.2555 \pm 0.0012_{stat} \pm 0.0021_{syst-stat} \pm 0.0050_{syst}} \tag{14a}$$

$$\boxed{\frac{\mathrm{BR}(K_S\to\pi^+\pi^-(\gamma))}{\mathrm{BR}(K_S\to\pi^0\pi^0)} = 2.2555 \cdot (1 \pm 0.0005_{stat} \pm 0.0009_{syst-stat} \pm 0.0022_{syst})}, \tag{14b}$$

where the first error is due to signal counts, the second one is from statistical fluctuations

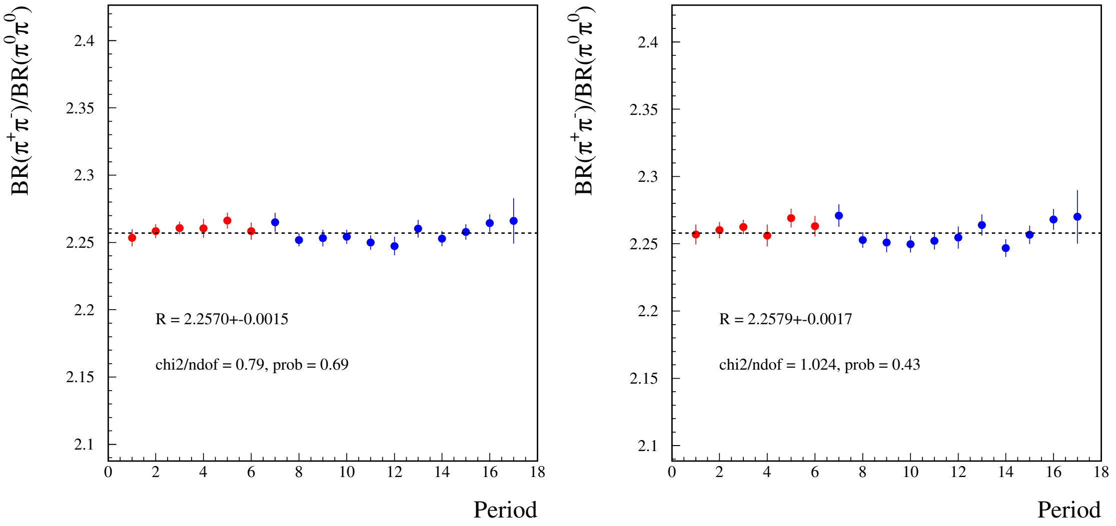

Figure 50: Ratio of $\mathrm{BR}(K_S \to \pi^+\pi^-(\gamma))/\mathrm{BR}(K_S \to \pi^0\pi^0)$ for a minimum K_{cr} energy of 125 MeV (left panel) and 200 MeV (right panel), as a function of the data taking period. The error bars represent the statistical error.

$K_{\rm cr}$ Energy cut	125 MeV	200 MeV	300 MeV
Source	Fractional statistical error, $\times 10^{-3}$		
Event count	0.34	0.40	0.54
Cosmic veto	0.14	0.18	0.26
Corrections	0.53	0.62	0.89
Total stat	0.64	0.76	1.1
Source	Fractional systematic error, $\times 10^{-3}$		
$\pi^0\pi^0$: Cluster counting	0.65	0.42	0.50
$\pi^0\pi^0$: Splitting	0.11	0.11	0.11
$\pi^0\pi^0$: Photon conversions	0.38	0.38	0.38
$\pi^0\pi^0$: Wrong K_S-$T_0^{\rm ev}$	0.60	0.60	0.61
$\pi^0\pi^0$: Background	0.35	0.14	0.04
$\pi^0\pi^0$: "Splash" events	0.13	0.09	0.07
$\pi^+\pi^-$: K_S-K_L interference	0.80	0.80	0.80
$\pi^+\pi^-$: $\epsilon_{\rm T0}$ correction	2.0	1.8	1.4
$\pi^+\pi^-$: Background	0.1	0.1	0.1
$\pi^+\pi^-$: Trigger	0.91	0.78	0.67
$\pi^+\pi^-$/$\pi^0\pi^0$: Accidental rate	0.47	0.48	0.52
$\pi^+\pi^-$/$\pi^0\pi^0$: f_n, P_n^{in}, P_n^{out} evaluation	0.67	0.53	0.45
$\pi^+\pi^-$/$\pi^0\pi^0$: ϵ_{cr}	0.39	0.62	0.44
$\pi^+\pi^-$/$\pi^0\pi^0$: FILFO	0.45	0.46	0.74
Total syst	2.8	2.5	2.2
Total	2.8	2.6	2.5

Table 10: Contributions to the statistical and systematic uncertainties are listed, for $K_{\rm cr}$ minimum energy of 125, 200 and 300 MeV.

of the various correction factors (second and third row of Tab.10), and the last one is the systematic error.

This has to be compared with the result that has been published analysing the year

$K_{\rm cr}$ energy cut (MeV)	125	200	300
Result	2.2574 ± 0.0025	2.2519 ± 0.0027	2.259 ± 0.004
χ^2/ndof	3.12/2		
$P(\chi^2)$	21%		

Table 11: Results from the analysis of 94 micro-periods with $K_{\rm cr}$ energy cuts of 125, 200, and 300 MeV. The statistical errors are shown. The χ^2 value for a fit to a constant and the associated probability is also listed.

2000 data sample [5]:

$$\frac{\mathrm{BR}(K_S \to \pi^+\pi^-(\gamma))}{\mathrm{BR}(K_S \to \pi^0\pi^0)} = 2.236 \cdot (1 \pm 0.0014_{stat} \pm 0.0037_{syst-stat} \pm 0.0057_{syst}) \quad (15)$$

The error was dominated by the systematic uncertainty on the ratio of tagging efficiencies (4.9×10^{-3}), which was computed by using the $K_{\rm cr}$ β^* spectrum on $\pi^+\pi^-$ events with the T_0 evaluated in the photon and pion hypotheses respectively. The systematic error was estimated in order to account for a possible bias related to the difference between the β^* spectrum for $\pi^+\pi^-$ and $\pi^0\pi^0$ events, both evaluated with a correct T_0 assignment (for further details refer to [7]).

This bias has been estimated by comparing in the present analysis the old method for the ratio of tagging efficiencies with the new one, which has a much smaller systematic uncertainty. The ratio of the two results, computed with $K_{\rm cr}$ minimum energy of 200 MeV(as in the published analysis), is $R_{tag}^{new}/R_{tag}^{old} = 0.994$. A bias in the old estimate of R_{tag} is therefore measured, with magnitude of the order of one σ_{syst} and capable to cover much of the difference between the present and the published measurement. Moreover the ratio of tagging efficiencies is the only relevant aspect of the analysis which has been changed respect to the published one.

Therefore when combining the present result with the published one, it is meaningful to consider the systematic error of the ratio of tagging efficiencies together with the statistical errors of both measurements:

$$R_{av}^{\pi\pi} = \frac{R_{old}^{\pi\pi}/\sigma_{old}^2 + R_{new}^{\pi\pi}/\sigma_{new}^2}{1/\sigma_{old}^2 + 1/\sigma_{new}^2}$$

where $\sigma_{old,new} = \sqrt{\sigma^2_{stat} + \sigma^2_{tag-syst}}$. We get $R^{\pi\pi}_{av} = 2.2549 \pm 0.0025$, with $\chi^2/ndof = 1.83$ and probability $P(\chi^2) = 18\%$. The correlated part of the systematic error has been averaged with the statistical errors. The final average with the old measurement is therefore:

$$\boxed{R^{\pi\pi}_{av} = 2.2549 \pm 0.0054.} \tag{16}$$

Acknowledgements

We are very greatful to M. Martini and S. Miscetti for the fruitful collaboration on the understanding of the systematics on $\pi^0\pi^0$ acceptance, and particularly for providing us the famous set of "Martini & Miscetti" correction factors.

References

[1] C. Gatti. MC generators for radiative kaon decays. KLOE note 194 (2004).

[2] C. Gatti. *Measurement of the branching fraction for the decay $K_S \to \pi e \nu$.* PhD thesis, Università degli Studi di Pisa, 2002.

[3] C. Gatti and T. Spadaro. Measurement of $\mathrm{BR}(K \to \pi^{\pm} e^{\mp} \bar{\nu}(\nu))$. KLOE note 176 (2002).

[4] C. Gatti and T. Spadaro. Measurement of the branching fraction and the charge asymmetry for the decay $K_S \to \pi^{\pm} e^{\mp} \bar{\nu}(\nu)$. KLOE memo 318 (2005).

[5] KLOE collaboration, A. Aloisio *et al. Phys. Lett.*, B538, 2002.

[6] KLOE collaboration, A. Aloisio, *et al. Phys. Lett.*, B535, 2002.

[7] T. Spadaro M. Palutan and P. Valente. Measurement of $\Gamma(K_S \to \pi^+\pi^-(\gamma))/\Gamma(K_S \to \pi^0\pi^0)$ with KLOE 2000 data. KLOE note 174 (2002).

[8] M. Martini and S. Miscetti. Determination of the probability of accidental coincidence between machine background and collision events and fragmentation of electromagnetic showers. KLOE note 201 (2005).

[9] M. Martini and S. Miscetti. A direct search for $K_S \to \pi^0\pi^0\pi^0$ decay with the kloe detector at dafne. KLOE note 200 (2005).

[10] T. Spadaro. *Studies of Ks decays at the Kloe Experiment.* PhD thesis, Università degli Studi di Roma "La Sapienza", 2001.

[11] D. E. Groom *et al.* The Review of Particle Physics. *Eur. Phys. J.*, C15, 2000.

[12] M. Adinolfi *et al.* The trigger system of the kloe experiment. *Nucl. Instrum. Meth.*, A492:134–46, 2002.

[13] S. Eidelman *et al.* The Review of Particle Physics. *Physics Letters B*, 592, 2004.